Hernández-Uribe David (Orcid ID: 0000-0002-5335-4131)

THE VERSATILITY OF PETROLOGICAL MODELING: THERMOBAROMETRY OF HIGH-PRESSURE METABASITES FROM THE RENGE AND SANBAGAWA BELTS AND PHASE EVOLUTION DURING WARM SUBDUCTION AT NANKAI

David Hernández-Uribe[1*] and Fabián Gutiérrez-Aguilar[2]

[1]*Department of Earth and Environmental Sciences, University of Michigan, Ann Arbor, MI, USA*

[2]*Facultad de Ingeniería, Universidad Nacional Autónoma de México, Ciudad Universitaria, CDMX, Mexico*

*Corresponding author: dav.hernandez.uribe@gmail.com

ABSTRACT

Petrological modeling is a powerful technique to address different types of geological problems via phase-equilibria predictions at different pressure–temperature–composition (P–T–X) conditions. In this contribution, we show the versatility of this technique by (1) performing thermobarometrical calculations using phase equilibrium diagrams to explore the petrological evolution of high-pressure (HP) metabasites from the Renge and Sanbagawa belts, Japan; and by (2) forward-modeling the mineral–fluid–melt evolution of the subducted fresh and altered oceanic crust along the Nankai subduction zone geotherm at the Kii peninsula, Japan. In the first case, we selected three representative samples from these metamorphic belts: a glaucophane eclogite and a garnet glaucophane schist from the Renge belt (Omi area) and a quartz eclogite

This is the author manuscript accepted for publication and has undergone full peer review but has not been through the copyediting, typesetting, pagination and proofreading process, which may lead to differences between this version and the Version of Record. Please cite this article as doi: 10.1111/iar.12406

This article is protected by copyright. All rights reserved.

Author Manuscript

Author Manuscript

from the Sanbagawa belt (Besshi area). In particular, we calculated the peak metamorphic conditions at ~2.0–2.3 GPa and ~550–630 °C for the HP metabasites from the Renge belt, whereas for the quartz eclogite, the peak equilibrium conditions were calculated at 2.5–2.8 GPa and ~640–750 °C. According to our models, the quartz eclogite experienced partial melting just after peak metamorphism. On the other hand, in terms of the petrological evolution of the basaltic uppermost portion of the oceanic crust during subduction along the warm Nankai geotherm, our models show that fluid release occurs at ~20–60 km, likely promoting high pore-fluid pressure, and thus, seismicity at these depths; dehydration is controlled by chlorite breakdown. Our petrological models predict partial melting at > 60 km, mainly driven by phengite and amphibole breakdown. According to our models, the melt proportion is relatively small, suggesting that slab anatexis is not an efficient mechanism for generating voluminous magmatism at the considered conditions. Modeled melt compositions correspond to high-SiO_2 adakites; these are similar to compositions found in the Daisen and Sambe volcanoes, in SW Japan. We posit that, while at the considered conditions melt migration may not occur, the modeled melts may serve as an analogue to explain adakite petrogenesis.

Keywords: phase equilibrium modeling, thermobarometry, Renge belt, Sanbagawa belt, Nankai, subduction, SW Japan

INTRODUCTION

The application of phase equilibrium modeling in metamorphic petrology is one of the greatest advances in recent decades and has now been established as a ubiquitous technique to address geological problems (Lanari et al., 2019; Powell et al., 2005; Spear et al., 2017; Yakymchuk,

Author Manuscript

2017). Via this technique, it is possible to define equilibrium mineral–fluid–melt relationships over a range of pressure and temperature (*P*–*T*) conditions for a whole-rock composition (*X*) (Hensen, 1971; Powell, 1978; Powell et al., 1998, 2005; Spear, 1988, 1995). Phase equilibrium modeling not only provides robust constraints on the *P*–*T* conditions of equilibration of a rock but also a wide range of associated petrological information such as mineral and bulk-rock densities at different *P*–*T*–*X* conditions (Powell and Holland, 2008, 2010; Yakymchuk, 2017). The theory behind this technique is beyond the scope of this paper and is not discussed here but can be found in different reviews (Lanari and Duesterhoeft, 2018; Powell et al., 2005; Powell and Holland, 2008).

The versatility of this technique allows performing thermobarometrical calculations as well as forward modeling of geological systems. In the first case, *P*–*T* conditions can be obtained by constructing phase diagrams for a particular bulk-rock composition, commonly referred to as pseudosections, isochemical phase diagrams, and/or phase equilibrium diagrams (Powell and Holland, 2008, 2010). By working backward, the *P*–*T* conditions can be refined by; for example, comparing measured vs. predicted mineral compositions and proportions within a calculated field of interest (Powell and Holland, 2008, 2010). Examples in the literature applying phase equilibrium modeling to do thermobarometrical calculations are vast (e.g., Baziotis et al., 2017; Cao et al., 2018; Dragovic et al., 2020; Groppo et al., 2015; Guevara et al., 2017; Gutiérrez-Aguilar et al., 2021; Hernández-Uribe et al., 2019; Klonowska et al., 2017; Massone, 2015; Li et al., 2020; Palin et al., 2013; Štípska and Powell, 2005; St-Onge et al., 2013; Wei et al., 2013; Weller et al., 2015; among many others). In the case of forward modeling, petrological calculations can be performed along a sequence of *P*–*T* points to determine paragenesis along a given *P*–*T*–*X* path. Therefore, it is possible to explore and evaluate the mineral–fluid–melt

Author Manuscript

evolution of different lithologies along different trajectories and shed light on important geological processes such as slab devolatilization, hydrothermal alteration of the oceanic floor, water transport to the mantle through time, intermediate-depth seismicity, and crustal formation and growth, just to mention some examples (Baxter and Caddick, 2013; Collins et al., 2015; Condit et al., 2020; Hernández-Montenegro et al., 2021; Hernández-Uribe et al., 2020; Kendrick and Yakymchuk, 2020; Konrad-Schmolke et al., 2011; Palin et al., 2017; Walters et al., 2020; among other examples).

Japan exposes some of the best studied and most classic high-pressure (HP) metamorphic belts worldwide and is one of the most seismic-active countries in the world. This unique place, therefore, represents a natural laboratory to show the versatility of phase equilibrium modeling. In this contribution, we selected two cases of studies to show how this technique can be used to address petrological questions. The first part of the paper addresses thermobarometrical questions using phase equilibrium diagrams and modeled mineral compositions to reevaluate the *P–T* evolution of the HP metamorphic rocks from the Late Paleozoic Renge belt and the Cretaceous Sanbagawa belt. These results are then compared with previous studies and discuss in terms of their importance in the understanding of the tectonothermal evolution of such metamorphic belts. The second part shows the potential of this technique to forward-model equilibria during subduction. We explored the petrological evolution of the subducted fresh and altered oceanic crust during subduction along the Nankai subduction *P–T* path. These results are further discussed in terms of their importance for seismogeneis and slab anatexis in Nankai subduction zone at the Kii peninsula.

METHODS

Author Manuscript

Thermobarometry

We selected two cases of study to perform thermobarometrical calculations via petrological modeling. One example corresponds to the Omi mélange of the Renge belt (Banno, 1958; Shinji and Tsujimori, 2019; Tsujimori, 2002) and the other to the well-known Sanbagawa belt (Figure 1; Itaya et al., 2011; Miyashiro, 1961). In both cases, we first calculated the phase equilibria and then compare published mineralogical and textural observations with our model predictions to put tighter constraints on the *P–T* evolution of these metamorphic belts.

In order to refine the HP–low-temperature (LT) evolution of the HP metabasites from the Renge belt, we selected two representative metabasite samples from the Omi area: a glaucophane eclogite, and a garnet glaucophane schist. The bulk-rock compositions used for calculating the phase equilibrium diagrams correspond to samples ECb and GG from Tsujimori (2002). Both types of lithologies are spatially related, and outcrop in the Yunotai Valley and interpreted by Tsujimori (2002) to record the same peak eclogite-facies metamorphism. On the other hand, to explore the HP evolution of Sanbagawa belt, we selected a kyanite-bearing quartz eclogite from the Gongen area (Besshi area). The bulk-rock composition used for calculating the phase equilibrium models correspond to sample GE1501a from Miyamoto et al. (2007) and Enami et al. (2019). All bulk-rock compositions are given in Table 1.

Mineral compositions used to constrain the *P–T* evolution of the samples from the Renge belt are from Shinji and Tsujimori (2019) and Tsujimori (2002), whereas for the Sanbagawa sample correspond to Miyamoto et al. (2007).

Models were constructed from 0.8–2.5 GPa and 450–650 °C for samples from the Renge belt whereas for the eclogite from the Sanbagawa belt, the model was calculated from 1.3–3.0

GPa and 550–800 °C. Calculated phase equilibria for the HP metabasites are shown in Figures 2 and 3, and a comparison with our results and previous works is shown in Figure 4.

Phase evolution during subduction

We apply forward petrological modeling to explore the mineral–fluid–melt evolution experienced by the basaltic uppermost portion of the oceanic crust during subduction along the Nankai subduction *P*–*T* path (Figure 1). For this, we used the thermal models from Abers et al. (2013) for the Kii peninsula at Nankai, and the N-MORB compositions from Gale et al. (2013) and the "supercomposite" compositions from Staudigel et al. (1996) (refer hereafter as "fresh MORB" and "altered OC", respectively), considered here as being representative of the subducted oceanic crust. The X_{Fe}^{3+} [$X_{Fe}^{3+} = Fe^{3+}/(Fe^{2+}+Fe^{3+})$] ratio for both compositions was set to 0.24, lying within the range defined by fresh basaltic glasses, different sections of the fresh and altered oceanic crust, and exhumed mafic eclogites (0.10–0.36; Berry et al., 2018; Rebay et al., 2010; Walters et al., 2020). Both bulk-rock compositions are given in Table 1.

Modeling of the melt trace elements was performed using the equation for modal melting of Shaw (2006) using mineral–melt partition coefficients from Bédard (2006). The subsolidus trace-element compositions of fresh MORB and altered OC were taken from Gale et al. (2013) and Staudigel et al. (1996), respectively. Here, we didn't consider the effects of dehydration on the budget of fluid-mobile elements through subduction. We envision that fluid-mobile elements, such as the LILE, will be depleted compared to the original compositions used here as a consequence of slab-top dehydration prior to melting. Therefore, the reported melt compositions should be slightly depleted than showed in our results. All modeled melt compositions are given in Table 2

Author Manuscript

Author Manuscript

Phase equilibria are shown using mode boxes in Figure 5, which show the calculated normalized volume proportions (vol. %) of all predicted phases (without H_2O) at each *P*–*T* point. Models were performed from 350 ºC and ~1.9 GPa to 750 ºC and ~2.8 GPa.

Modeling setup and uncertainties

All phase equilibria were calculated using Theriak-Domino (de Capitani and Brown, 1987; de Capitani and Petrakakis, 2010) and the internally consistent thermodynamic data set ds62 (Holland and Powell, 2011) in the $MnO–Na_2O–CaO–K_2O–FeO–MgO–Al_2O_3–SiO_2–H_2O–TiO_2–O_2$ (MnNCKFMASHTO) system. The following activity–composition (*a*–*X*) relations for solid-solution phases were used: clinopyroxene (omphacite model), clinoamphibole, and melt (Green et al., 2016); garnet, biotite, muscovite–paragonite, and chlorite (White et al., 2014); epidote (Holland and Powell, 2011); plagioclase (Holland and Powell, 2003); magnetite–spinel (White et al., 2002); and ilmenite–hematite (White et al., 2000). Pure phases included talc, lawsonite, kyanite, quartz, rutile, titanite, and albite. Aqueous fluid was considered pure H_2O and in excess in all models at subsolidus conditions. In models shown in Figures 5–7, we considered H_2O excess up to the point of initial melting, afterward, the H_2O content was fixed to allow minimal saturation (< 2 vol. % of H_2O) at the conditions where the modeled geotherm crosses the wet solidus.

The main uncertainties associated with phase equilibrium modeling are systematic uncertainties (also referred as “bias”; Powell, 1985; Powell and Holland, 2008) and random uncertainties (Guevara and Caddick, 2016; Lanari and Engi, 2017; Powell and Holland, 2008; Palin et al., 2016). The former is related to uncertainties in the thermodynamic data and *a*–*X* models (Powell, 1985; Powell and Holland, 2008), which dictate to what degree phase

Author Manuscript

assemblages and mineral compositions can be accurately reproduced. The second type of uncertainties mainly comprises geological uncertainties (Guevara and Caddick, 2016; Lanari and Engi, 2017; Palin et al., 2016). In this case, the accuracy of the modeling is affected by introducing errors associated with uncertainties due to the choice of reactive/effective bulk-rock compositions, the extent of equilibrium of a phase assemblage, and phase (e.g., garnet and melt) fractionation during the *P–T* evolution, to mention some (for a detail discussion of uncertainties see Powell and Holland, 2008; Yakymchuk, 2017). Furthermore, analytical errors associated with electron microprobe analysis can introduce extra uncertainties when calculating *P–T* estimates using compositional isopleths; for instance, error propagation of a mineral compositions may lead to ±0.01 atoms per formula unit difference, which, when compared to modeled isopleths translate to errors in the *P–T* estimates.

In this work, all our results are affected by both systematic and geological uncertainties which are difficult to assess; thus, in all our models, uncertainties are estimated to be—at least—around ±1 kbar and ±50 °C at the 2σ level (Powell and Holland, 2008).

THERMOBAROMETRY OF HP METABASITES FROM JAPAN

Geological settings

The Renge belt

The Late Paleozoic Renge Belt and its equivalent units occur sporadically throughout SW Japan (Figure 1; Tsujimori and Itaya, 1999). The Renge belt consists of antigorite serpentinite-matrix mélange with HP rocks, mainly clastic sequences and metasedimentary schists, referred as the Renge Schists (Banno, 1958; Kunugiza et al., 2004; Tsujimori, 2002; Tsujimori and Harlow, 2017; Yamada et al., 2019; Yoshida et al., 2021). The Omi (Itoigawa-Omi) area has been well

known as a locality of gem-quality jadeitite (Tsujimori and Harlow, 2017). Glaucophane eclogites and garnet glaucophane schists occur as layers within paragonite-bearing metasedimentary schists in the Omi area of the Renge schists (Tsujimori, 2002; Tsujimori and Matsumoto, 2006).

Tsujimori (2002) provided a detailed petrological study of the metamorphic evolution of these metabasites and proposed three different metamorphic stages for the HP–LT metamorphism of the area. The prograde mineral assemblage is constrained by inclusions of glaucophane + epidote + titanite + albite + quartz in garnet. This prograde blueschist-facies stage is broadly constraint to ~0.8–1.6 GPa and ~350–550 °C based on glaucophane + epidote paragenesis stable in the petrogenetic grid calculated by Evans (1990). The peak metamorphic eclogite-facies stage is represented by the assemblage garnet + omphacite + glaucophane + epidote + phengite + rutile +quartz. Garnet–omphacite–phengite conventional thermobarometry (Carswell et al. (1997) and Krogh (1988) calibrations) constrain the peak metamorphism at ~1.8–2.0 GPa and ~550–600 °C. Breakdown textural features suggest that the retrograde evolution is characterized by the late-stage mineral assemblage glaucophane + epidote + chlorite + titanite + albite + quartz + calcite; a recent study by Shinji and Tsujimori (2019) found late-stage pumpellyite coexisting with glaucophane. Similar to the prograde mineral assemblage, the *P–T* conditions were constrained using petrogenetic grids (Evans, 1990) by Tsujimori (2002).

The Sanbagawa belt

The late Cretaceous Sanbagawa belt (Figure 1) is a NE–SW trending belt extending for over ~800 km through Japan (Miyashiro, 1961; Matsumoto et al., 2003). The belt consists in a coherent array of HP metaigneous and metasedimentary bodies with minor calcareous and

Author Manuscript

ultramafic rocks (Banno and Sakki, 1989). This array has been interpreted as an accretionary complex formed during subduction at the eastern margin of Eurasia (Wallis et al., 2009). The highest-grade portions of the Sanbagawa metamorphic belt are exposed in the Besshi area, in central Shikoku; the eclogite-facies portion in the Besshi area consists of the Iratsu and the ultramafic Higashi-Akaishi bodies, and the Seba and Tonaru metabasites and schists (Aoki et al., 2020a,b; Aoya et al., 2001; Enami et al., 2004; Hattori et al., 2010; Kouketsu et al., 2010; Miyagi and Takasu, 2005; Miyamoto et al., 2007; Ota et al., 2004; Weller et al., 2015).

In the northeastern limit of the Higashi-Akaishi, a small quartz-rich eclogitic body separates the Higashi-Akaishi peridotite from the Iratsu HP metabasites (Enami et al., 2004). This body has been described in detail by Miyamoto et al. (2007) and Enami et al. (2019). The peak eclogite-facies paragenesis comprises garnet + omphacite + phengite + kyanite + quartz; thermobarometrical estimates indicate that this lithology experienced peak eclogite-facies conditions of 2.3–2.4 GPa and 675–740 °C—the highest recognized in throughout the Sanbagawa belt (Miyamoto et al., 2007). Prograde inclusions in garnet include amphibole (glaucophane, barroisite, and pargasite), paragonite, and phengite (Miyamoto et al., 2007). Textural retrograde features include amphibole + plagioclase symplectites around omphacite, and fine-grained paragonite and phengite around kyanite (Miyamoto et al., 2007).

Results

Glaucophane eclogite (Renge belt)

The phase relations calculated for the glaucophane eclogite are shown in Figure 2a,b. The interpreted peak paragenesis, garnet–omphacite–glaucophane–epidote–phengite–rutile–quartz is calculated to be stable at ~1.8–2.3 GPa and ~565–620 °C. The peak paragenesis field is limited

Author Manuscript

Author Manuscript

at lower pressures and higher temperatures by the glaucophane-hornblende solvus, at higher pressures and lower temperatures by lawsonite-bearing assemblages, at lower *P–T* conditions by omphacite-free assemblages, and by kyanite-bearing assemblages at higher temperatures.

For this sample, garnet and amphibole compositional isopleths were used to delimit the peak conditions within interpreted peak paragenesis field. The occupancy of Na in the crystallographic site "B" (Na_B) was used as a proxy to discriminate between different amphiboles (e.g., glaucophane vs hornblende, *sensu lato*) and compared with the observed compositions in the sample. The observed matrix glaucophane's Na_B content (>1.8 pfu) lies within the peak paragenesis field narrowing, it to ~2.0–2.3 GPa and ~570–630 °C. Furthermore, the observed garnet's rim grossular and pyrope (grs = 0.28–0.32 and prp = 0.10–0.12) compositional isopleths closely approach each other within the area defined by the glaucophane composition suggesting that the peak metamorphism likely occurred close to such *P–T* conditions.

While the bulk-rock composition may have varied through the entire metamorphic evolution of the glaucophane eclogite (e.g., due to fluid availability, Giraud et al., 2001), insights from the presence of some phases provide rough *P–T* constraints on the prograde and early-retrograde evolution of the rock. For instance, the set of inclusions within garnet (i.e., glaucophane, titanite, and albite) indicates that the prograde conditions might have been close to < 0.9 GPa and < 485 °C; however, the lack of biotite as inclusion in garnet suggests pressures >1.2 GPa. Therefore, the preferred *P–T* conditions of this stage are ~1.2 GPa and < 485 °C. Omphacite and rutile inclusions in garnet's rim suggest that the later prograde path evolve through such stability field. On the other hand, the presence of chlorite, titanite, and albite and

the lack of biotite roughly constrains the retrograde part of the path at least to ~0.9 GPa and ~500 °C.

Garnet glaucophane schist (Renge belt)

The phase relations calculated for the garnet glaucophane schist are shown in Figure 2c,d. The phase equilibrium diagram calculated for the garnet glaucophane schist shows that the interpreted peak paragenesis, garnet–glaucophane–epidote–phengite–rutile–quartz, is stable at ~1.7–2.2 GPa and ~ 550–590 °C. This mineral stability field is limited at higher *P–T* conditions by omphacite-bearing assemblages, at lower temperatures by lawsonite-bearing assemblages, at lower *P–T* conditions by chlorite-bearing stability fields, and by the glaucophane-hornblende solvus at higher temperatures.

Garnet composition analyses for this sample are not available in the literature, so we only use glaucophane's Na_B isopleths to delimit the peak *P–T* conditions within interpreted peak paragenesis field. The calculated glaucophane's Na_B isopleths generally yield lower Na_B contents than the observed in the garnet glaucophane schist (Na_B > 1.8 pfu), although relatively similar values (Na_B >1.7 pfu) lie within the peak stability field at ~2.0–2.1 GPa and ~550–565 °C, suggesting that peak metamorphism occurred close to such *P–T* conditions.

The prograde history of the garnet glaucophane schist is constrained by glaucophane and rutile inclusions within garnet, limiting the earlier part of the path to > 1.5 GPa and > 500 °C. Secondary chlorite and titanite constrain the retrograde part of the path to at least ~1.4 GPa and ~540°C, although biotite is not found in the sample.

Quartz eclogite (Sanbagawa belt)

Author Manuscript

Author Manuscript

The phase relations calculated for the quartz eclogite are shown in Figure 3a,b. The interpreted peak paragenesis, garnet–omphacite–phengite–kyanite–quartz, is calculated to be stable at 1.9–2.9 GPa and ~610–800 °C. The peak mineral assemblage field is limited at higher pressures and lower temperatures by lawsonite-bearing assemblages, and by suprasolidus assemblages at higher temperatures. At lower pressures, the peak assemblage field is limited by amphibole–epidote–paragonite assemblages. The peak assemblage field limits at higher pressures with coesite-bearing assemblages.

The peak paragenesis field expands over a large *P*–*T* range, extending up to ultra-HP conditions. Complex garnet zoning in the sample (Enami et al., 2019) precludes constraining the peak *P*–*T* conditions using garnet compositional isopleths. Thus, omphacite and phengite compositional isopleths were used instead to delimit the peak conditions within the relatively large field. The observed Si pfu in phengite in matrix (Si = ~3.29–3.34 pfu) and Al pfu in omphacite (Al = ~0.50 pfu) lie within the peak mineral assemblage field, further suggesting that peak conditions may have occurred close to ~2.5–2.8 GPa and ~640–750 °C.

The prograde evolution of the quartz eclogite is qualitative constrained by Na- and Na-Ca amphibole, paragonite, and phengite inclusions within garnet, suggesting that the prograde paths evolved through such stability fields. The presence of secondary amphibole, epidote, and paragonite constrain the earlier part of the retrograde conditions to suprasolidus conditions at ~1.3–1.7 GPa and ~620–690 °C. While melting during decompression likely changed the effective bulk-rock composition, we posit that the overall topology of the phase equilibria may have not been strongly affected such that the proposed *P*–*T* conditions of amphibole–epidote–paragonite stability field at suprasolidus condition may be relatively accurate.

Author Manuscript

P–T evolutions of the HP metabasites from the Renge (Omi) and Sanbagawa (Besshi) belts revisited

Figure 4 summarizes the *P–T* results for the HP lithologies modeled in this contribution and shows thermobarometrical estimates from other relevant studies. The peak *P–T* conditions shown in this figure correspond to the conditions narrowed by the modeled compositional isopleths as well as the observed mineral assemblage fields; only the former are discussed below.

The Renge belt (Omi area)

The prograde paths obtained in this contribution for the glaucophane eclogite and the garnet glaucophane schist are parallel to each other and are essentially the same within uncertainties related with the modeling, although the path for the glaucophane eclogite is ~40 °C hotter. The proposed prograde path for these metabasites follows a linear gradient d*T*/d*P* of = ~71–114 °C/GPa and is relatively similar to previous estimates for the same rocks (Tsujimori, 2002; Tsujimori and Matsumoto, 2006).

The peak *P–T* conditions for both samples calculated here are essentially the same within uncertainties, although they differ slightly from each other; the pressure for the garnet glaucophane schist is similar to the glaucophane eclogite but the temperature is ~40 °C higher. In both cases, the pressure calculations are ~0.3 GPa higher than estimated in previous works (Tsujimori, 2002; Tsujimori and Matsumoto, 2006) but the temperature is within previous estimates. Furthermore, our calculations for the glaucophane eclogite yields higher peak *P–T* conditions (i.e., ~2.0–2.3 GPa and ~570–630 °C) than previous estimates for the same lithology (~1.8–2.0 GPa and ~550–600 °C; Tsujimori, 2002; Tsujimori and Matsumoto, 2006). Previous

works suggest that the garnet glaucophane schist experienced coeval eclogite-facies metamorphism to the glaucophane eclogite but lack of omphacite due to differences in the bulk-rock composition (Tsujimori, 2002). As shown in our results for the garnet glaucophane schist, the interpreted peak paragenesis field is constrained at slightly lower pressures than the omphacite-bearing assemblages (Figure 2c). If the presence of omphacite was controlled by the bulk-rock composition, then the observed paragenesis in the garnet glaucophane schist (i.e., omphacite-free) would be stable at the same *P–T* conditions as the peak paragenesis in the glaucophane eclogite *P–T* diagram; yet the omphacite-in line is located at relatively similar *P–T* conditions in both petrological models (Figures 2a,c), suggesting that the presence (or lack thereof) omphacite may not be explained by compositional differences. Although the garnet glaucophane schist is compositionally different from the glaucophane eclogite (Table 1), we argue that either garnet glaucophane schist never reached eclogite-facies conditions or that if the rock did experience such *P–T* conditions, omphacite was completely consumed during exhumation; from these, we favor the former hypothesis.

The retrograde part of the paths evolves from the obtained peak conditions to ~0.9 GPa and ~500 °C for the glaucophane eclogite and ~1.4 GPa and ~540 °C garnet glaucophane schist. Both retrograde paths follow the same general trend although garnet glaucophane schist stops recording *P–T* conditions at earlier stages. According to our models, the retrograde path evolves through the stability field of Na-Ca and Ca amphiboles during exhumation to finally reach the actinolite stability field at greenschist-facies. The presence of actinolite replacing glaucophane in natural samples (Tsujimori, 2002; Shinji and Tsujimori, 2019) further supports the general trend of the proposed *P–T* path. Shinji and Tsujimori (2019) constrain the late-retrograde conditions to the pumpellyite stability field at ~0.6–0.7 GPa and ~300 °C, suggesting cold exhumation.

Author Manuscript

Author Manuscript

The Sanbagawa belt (Besshi area)

Our obtained prograde part of the *P–T* path is qualitative constrained by amphibole, paragonite, and phengite inclusions in garnet. The obtained prograde path extends to lower pressures as the stability fields of such set inclusions are relatively large, but the amphibole inclusion compositions (Na- and Na-Ca amphibole) delimit the start of the path to ~1.6 GPa and ~560 °C. The proposed prograde path for the quartz eclogite follows a d*T*/d*P* linear gradient of = ~114 °C/GPa. While not genetically related with the modeled quartz eclogite in our work, the proposed prograde *P–T* path for other Besshi HP metabasites (e.g., Weller et al., 2015) is less steep and slightly hotter than proposed and strongly differs with proposed widely open *P–T* path loops (Aoya et al., 2001).

Our petrological models for the quartz eclogite yield relatively similar peak *P–T* conditions (i.e., 2.5–2.8 GPa and ~640–750 °C) to previous estimates for the same lithology from Ota et al. (2004) and Miyamoto et al. (2007). Our calculated pressures are ~0.4 GPa higher, whereas the calculated temperatures are within the estimates of those studies. On the other hand, our obtained peak conditions for the quartz eclogite clearly differ from all the *P–T* estimates from other eclogite types of the Sanbagawa belt (e.g., Aoya et al., 2001; Endo and Tsuboi, 2013; Matsumoto et al., 2003; Ota et al., 2004; Weller et al., 2015), except for the jadeite-bearing kyanite eclogite from eastern Iratsu, which yield similar pressures but significantly lower temperatures (i.e., ~570–610 °C; Endo and Tsuboi, 2013). In particular, the calculated *P–T* conditions of the quartz eclogite are ~0.2 GPa and ~100 °C higher than estimates for Eastern Iratsu eclogites and ~0.8 GPa and ~150 °C higher than *P–T* conditions reported for eclogites from Western Iratsu (Endo et al., 2012; Endo and Tsuboi, 2013).

Author Manuscript

The retrograde part of the path evolves from the obtained peak conditions to ~1.3–1.7 GPa and ~620–690 °C, where amphibole, epidote, and paragonite are stable. The proposed retrograde path for the quartz eclogite follows a similar and parallel d*T*/d*P* gradient to the proposed prograde path and, importantly, crosses the modeled solidus during decompression. This indicates that the quartz eclogite partially melts during the early retrograde stage. Textural evidence suggests that the omphacite and kyanite are replaced by fine-grained amphibole and paragonite (Miyamoto et al., 2007), indicating that the retrograde path further evolves towards the paragonite stability fields. Arakawa et al. (2013) suggest that the quartz eclogite of this locality experienced partial melting after *c.* 10 Myr of peak metamorphism, supporting our calculated phase equilibria. The retrograde path obtained here significantly differs from the proposed for eclogites from eastern and western Iratsu (Endo and Tsuboi, 2013 and references therein) in that our modeled path is ~60 °C hotter. On the other hand, our path follows an overall similar trend to the proposed for the Higashi-Akaishi peridotite and associated eclogites (Ota et al., 2004), although our path is ~40 °C colder closer to peak conditions.

PETROLOGICAL MODELING OF THE SUBDUCTED OCEANIC CRUST IN THE NANKAI SUBDUCTION ZONE

In this section, we forward-model the mineral–fluid–melt evolution experienced by the fresh and altered uppermost portion of the oceanic crust during subduction along the Nankai subduction *P–T* path at the Kii peninsula.

Fresh portion of the upper oceanic crust

Author Manuscript

The phase evolution of a fresh MORB during subduction is shown in Figure 5a. At the onset of subduction, the metabasite stabilizes greenschist-facies assemblages, where the most abundant phases are amphibole, epidote, albite, and chlorite (~90 vol. %). As our model includes Mn, the garnet stability expands to the beginning of the path, although with negligible proportions (<1 vol. %). With increasing *P–T* conditions, albite and chlorite are consumed at ~0.9 GPa and 460 ºC and ~1.1 GPa and 500 ºC, respectively. At this point, the H_2O content within hydrous phases slightly decreases from ~3.0 to ~1.8 wt. % H_2O. Here, the metabasite show amphibolite-facies assemblages. Clinopyroxene stabilizes slightly before the consumption of biotite at ~1.2 GPa and 530 ºC. At earlier stages of subduction, biotite is stable, and in the latter stages of the *P–T* evolution, muscovite stabilizes. With increasing *P–T* conditions, titanite is completely consumed at ~1.4 GPa and 620 ºC stabilizing rutile. The mineral assemblage after rutile stabilization comprises omphacite, amphibole, quartz, epidote, garnet, and phengite, where amphibole dominates the assemblage. Importantly, amphibole and epidote are stable through the entire *P–T* path, generally decreasing in proportion at the final stages of the modeling. The H_2O content in the metabasite at ~1.6 GPa and 680 ºC is ~1.2 wt. % H_2O.

The HP metabasite melts during subduction at ~1.6 GPa and 680 °C. Phengite and H_2O are consumed at the solidus, and the subsequent partial melting is driven by quartz, amphibole, and clinozoisite consumption. At suprasolidus conditions, garnet and clinopyroxene increase their proportions as *P–T* increases. The amount of melt generated during subduction in the Nankai subduction zone is always < 10 vol. %. The melt compositions generated during melting of the fresh MORB are shown in Figure 6 and given in Table 2. These melts have SiO_2 = 71.82–72.75 wt. % and MgO < 1 wt. %. The chondrite-normalized rare earth element (REE) patterns are strongly fractionated (La/Yb = 33–61), show positive Eu negative anomalies, and

are characterized by high Sr/Y ratios (Sr/Y = 63–111) (Figure 6b,c). At the end of the modeled path, the solid assemblage comprises ~50 vol. % garnet and omphacite, retaining ~0.6 wt. % of H_2O.

Altered portion of the upper oceanic crust

Phase evolution of altered OC during subduction is shown in Figure 5b. From ~0.6–0.8 GPa and 350–430 ºC, the metamorphosed uppermost altered portion of the crust stabilizes greenschist-facies assemblages, dominated by albite, epidote, amphibole, chlorite, and biotite (~98 vol. %). Similar to the fresh MORB, garnet stability expands to the beginning of the path, although with negligible proportions (<1 vol. %) due to the Mn consideration. Epidote is stable throughout the entire path with ~30 vol. % at earlier stages and ~10 vol. % at the end of modeling. Amphibole stabilizes at ~0.6 GPa and 360 ºC, partially consuming chlorite. Chlorite is completely consumed at ~1.0 GPa and 490 ºC stabilizing clinopyroxene and increasing garnet proportion; this reaction causes a significant H_2O-decrease from ~3.0 to ~1.9 wt. % H_2O. Here, the altered metabasite displays amphibolite-facies assemblages. Biotite is stable at early stages of subduction and white mica in the later portions of the model. With increasing *P–T* conditions, the progressive consumption of amphibole and phengite cause a decrease in the H_2O content from ~1.5 wt. % to ~0.5 wt. % H_2O at the end of the model. Titanite is completely consumed at ~1.4 GPa and 630 ºC stabilizing rutile. At ~1.6 GPa and 680 ºC, the altered metabasite is mainly composed of garnet, omphacite, amphibole, epidote, phengite, quartz, and rutile. At the solidus (i.e., ~1.7 GPa and ~690 °C), H_2O is consumed, and in contrast to the fresh MORB, phengite remains stable at suprasolidus conditions. The melt fraction increases as quartz, amphibole, and clinozoisite are

Author Manuscript

consumed. At suprasolidus conditions, garnet and clinopyroxene increase their proportions as *P–T* increases.

Similar to the previous example, the melt fraction is never <10 vol. % of the assemblage. The melt compositions generated during melting of the altered OC are shown in Figure 6 and given in Table 2. The melts generated in this example are almost identical to the MORB-derived model in terms of major elements; melts in this example show SiO_2 = 71.79–72.73 wt. % and MgO < 1 wt. % (Figure 6a; Table 2). The chondrite-normalized REE patterns are strongly fractionated (La/Yb = 32–56), show positive Eu negative anomalies, and are characterized by high Sr/Y ratios (Sr/Y = 119–209) (Figure 6b,c). At the end of the modeled path, the solid assemblage comprises ~60 vol. % garnet and omphacite.

Implications for the Nankai subduction zone

Slab-top dehydration

Our petrological models for both fresh and altered oceanic crust show that chlorite breakdown (Figures 4 and 5) plays the most important role in the dehydration of the oceanic slab-top during subduction at Nankai. The first garnet appearance in the mineral assemblage promotes slight chlorite consumption and thus promotes fluid release, although the most important fluid loss event occurs when chlorite is completely consumed at ~30–35 km depth (Figure 5). After chlorite breakdown at those depths, fluid is released gradually as amphibole and clinozoisite are consumed to form garnet and clinopyroxene. This is in good agreement with other models showing the importance of chlorite dehydration in warm subduction zones (e.g., Baxter and Caddick, 2015; Hernández-Uribe and Palin, 2019a).

Author Manuscript

Author Manuscript

Most of the dehydration of the fresh and altered OC of the subducting oceanic crust occurring along the Nankai slab-top path occur within ~20–60 km depth. This depth range is in great agreement with the depths where non-volcanic tremor (NVT) and slow-slip events (SSE) occur according to different compilations for this region (Figure 7). Importantly, the depths where chlorite breaks down in our models (~ 30–35 km) perfectly match with one of the occurrence peaks of the NVT at shallower depths. Furthermore, our results are in agreement with the modeled overall fluid-release depths of Abers et al. (2013) and Tatsumi et al. (2020), although our models suggest that more water is being released in this subduction segment. On the other hand, our results differ from those of Condit et al. (2020) and Kimura et al. (2014) in that our modeled dehydration occurs shallower than in their models, which occur at > 60 km depth. Most models that explain different slip behaviors require the presence of high pore-fluid pressure within the slab–mantle interface. The origin of these fluids is still debated (e.g., Fagereng et al., 2018; Hyndman et a., 2015); notwithstanding, the good match between chlorite breakdown predicted by our models and the NVT and SSE occurrence in the Kii peninsula suggest an *in situ* origin for the fluid that promotes high pore-fluid pressures at such depths.

Slab-top melting

Our models show the compositions of the initial melts formed during subduction along a warm geotherm. As expected for melts derived from slab anatexis, our calculated melt compositions show adakitic signatures (Defant and Drummond, 1990; Moyen, 2009; Hernández-Uribe et al., 2020) and are further classified as high-SiO_2 adakites (Martin et al., 2005) (Figure 6).

Anatexis is driven by the consumption of hydrous minerals, specifically amphibole (Figure 5). The solid residuum at suprasolidus conditions is not eclogite *sensu stricto* as the

Author Manuscript

assemblages are dominated by amphibole and comprise only < 60 vol. % of garnet + omphacite in both examples analyzed here (Figure 5). However, the melt's geochemical signature still displays high Sr/Y and La/Yb ratios as garnet and amphibole are present. Thus, we suggest that in order to exert a high Sr/Y signature to the melt, the source does not necessarily need to be a fully-eclogitized oceanic crust. Petrological models show that anatexis of a fully-eclogitized (*sensu stricto*) pristine oceanic crust results in melts with considerably higher Sr/Y ratios than shown here (Fig. 6; Hernández-Uribe et al., 2020).

The calculated compositions from the MORB and altered OC melts are relatively similar, although the altered OC-derived melts are slightly depleted in heavy-REE compared to melts derived from fresh MORB. Similarly, the altered OC-derived melts have higher Sr/Y and Y contents. We suggest that these differences are accounted by the difference in amphibole (dV = ~15 vol. % at 700 °C) and garnet (dV = ~8 vol. % at 700 °C) proportions at the same *P*–*T* conditions in both considered compositions, as well as the original protolith heavy-REE concentrations.

Slab-top melting in our results occurs at ~57 km. Petrological models for both the fresh MORB and altered OC predict melt proportion of < 10 vol. % of the phase assemblage. Relatively few models for the Nankai subduction zone account for the presence of melt (e.g., Kimura et al., 2014). In their study, the geotherm crosses the solidus at depths ~90 km and produces significantly more melt fractions than in our models. According to our results, we consider melt migration unlikely at the explored depths, and if it occurs, relatively small volumes can migrate because our predicted melt fractions are lower than the ~20 vol. % threshold required for melt loss (Rushmer, 1995; Vigneresse et al., 1996). However, at greater depths (not

modeled), the melt will likely accumulate and further migrate to generate voluminous magmatism.

Our modeled major and trace-element compositions are similar to quaternary adakites found in the Daisen and Sambe volcanoes in SW Japan (Figure 6; Morris, 1995; Kimura et al., 2014). Modeled compositions show similar REE patterns and almost identical Sr/Y (Figure 6), and similar Y and Yb contents to rocks found at such volcanoes. The petrogenesis of such adakites is still debated; some studies suggest that the Daisen and Sambe adakites form due to slab-melting of the subducting Philippine Sea crust (Morris, 1995) and/or slab melts that interacted with the asthenosphere (Kimura et al., 2005, 2014), whereas other studies suggest that they form by the partial melting of the overriding Eurasian lower crust (Zellmer et al., 2012). Our petrological models show that during warm subduction, melts with almost identical Sr/Y and REE signatures can form. Thus, we posit that the slab-melting played a crucial role in the formation do the Daisen and Sambe adakites, and little to no mantle interaction is needed to provide the observed Sr/Y and REE signatures.

DISCUSSION

Thermobarometry

In this contribution, we show how applying petrological modeling is useful to constrain the *P–T* evolution of HP metamorphosed rocks (Figures 2–4), and to evaluate the phase changes that occur during subduction as wells as compositional evolution of melt generated during subduction (Figures 5–7).

In contrast to conventional thermobarometry, petrological modeling provides context to minerals that are not interpreted to represent part of a determined paragenesis. For example, we

Author Manuscript

Author Manuscript

constrained the earlier part of the metamorphic histories by using mineralogical and textural observations such as the mineral inclusions in garnet cores. Similarly, the retrograde evolution was roughly constrained by textural relations between the interpreted peak and retrograde phases. On the other hand, peak *P–T* conditions were calculated by coupling mineral compositions as well as the observed peak paragenesis; for this, we interpreted that the observed mineral compositions (i.e., garnet—when available—and glaucophane rims) to be representative of peak conditions and thus record the peak eclogite-facies metamorphism. While using *P–T* paths derived from a single model to describe the complete *P–T* evolution of a rock is not recommended as the equilibration volume at different scales likely changes through time (e.g., Guevara and Caddick, 2016; Lanari and Engi, 2017; Palin et al., 2016), the overall trend is still useful to shed light into the evolution of metamorphic rocks.

Overall differences between previous *P–T* calculations and our results are likely explained by the different thermobarometrical approaches. For instance, previous works used petrogenetic grids and conventional thermobarometers (Miyamoto et al., 2007; Ota et al., 2004, Tsujimori, 2002), whereas in this contribution we use phase equilibrium modeling (Figures 2–4). All of these techniques are affected by different uncertainties. For instance, conventional thermobarometers are susceptible to large uncertainties such as the ones associated with Fe^{3+}detemination in a phase; for instance, in clinopyroxene which can lead to uncertainties up to ±300 °C (Ravna, 2003; Proyer et al., 2004). Ferric iron also complicates calculations via phase equilibrium modeling as getting an accurate X_{Fe}^{3+} is difficult because the oxidation state during metamorphism may be unknown. Similarly, calculations with conventional thermobarometry can also be affected by modifications of the mineral compositions after peak metamorphism, such as diffusion (Pattinson et al., 2003); for instance, a sensitivity test of the garnet–omphacite

Author Manuscript

thermometer in eclogites suggest that diffusion can affect the *P–T* calculations by ± 0.4 GPa and ± 100 °C (Hernández-Uribe et al., 2018). While diffusion does not affect the results from modeling, it affects the minerals used to compare with model predictions (i.e., the compositional isopleths), inhibiting a refinement of the *P–T* conditions as our model for the quartz eclogite. For example, modeled garnet isopleths at peak *P–T* conditions should be relatively higher than the analyzed garnet composition, as this one has been affected by diffusion relaxation (if high-*T* is reached; Caddick et al., 2010; Konrad-Schmolke et al., 2005) Some of these issues are easier to approach by phase equilibrium modeling; for example, the Fe^{3+} content can be estimated by (1) using the Fe^{3+} content from known similar and relevant lithologies (e.g., Wei and Duan, 2018); and (2) reproducing the observed the overall phase equilibria and proportions of the sample of interest (e.g., Hernández-Uribe and Palin, 2019b; Massonne, 2012); this can be done via the construction *T–X* or *P–X* phase diagrams (Diener and Powell, 2010).

We thus suggest that in order to better understand the *P–T* evolution of a metamorphic rock, it is recommended to complement petrological modeling with other thermobarometrical techniques as this are independent of the data and assumptions made in this type of modeling, as also suggested by other workers (e.g., Hacker, 2006; Hernández-Uribe et al., 2018; Powell and Holland, 2008; Štípska et al., 2005; Wei and Clarke, 2011).

Phase evolution during subduction

In this contribution, we also show how petrological modeling can constrain the depths of slab-top dehydration and melting during subduction in the Nankai subduction zone. Our models indicate that the depth of the chlorite-driven dehydration is in good agreement with the depths where NVT and SSE occur in the Kii peninsula, Japan. Furthermore, our petrological models

Author Manuscript

suggest that adakitic melts form during melting of the oceanic crust; such calculated melt major and trace-element compositions are in good agreement with quaternary volcanism in SW Japan.

In general, our results are similar to the fluid release depths predicted by Abers et al. (2013) and Tatsumi et al. (2020) but differ from those of Condit et al. (2020) and Kimura et al. (2014.) The latter ones predict different dehydration depths, and in the case of Kimura et al. (2014) models, slab-top melting occurs at greater depths and magmatism is more voluminous than our prediction. All these differences may be explained by different thermodynamic databases and a–X models used in the petrological modeling. Moreover, differences can also be accounted for by the different geotherms used in the different works. For example, Condit et al. (2020) use the Peacock (2009) model, which uses modern convergence rates; by contrast, our models are based on the Abers et al. (2013) thermomechanical model, which uses a slower rate (2 cm/yr over a time span of 20 Myr) to approximate any changes in subduction rate through time.

Our results describe what would occur during oceanic subduction if equilibrium was reached during metamorphism. As mention in the Methods section, all our model results are subject to different types of uncertainties. For example, one important assumption made here is that the phase assemblages formed and evolve through a series of equilibrium states until peak conditions are reached (Powell et al., 2005; Powell and Holland, 2008, 2010); this assumption is only an end-member on a spectrum of possible scenarios found in nature, although it is likely true in hydrated rocks, as fluids drive reactions between phases in a system, promoting equilibrium (Guiraud et al., 2001; Powell et al., 2005). On the other hand, when fluid is absent or when metamorphism occurs during fluid undersaturated conditions, metabasites—and any type of metamorphic rock—are expected to experience only limited mineral reactions (Guiraud et al.,

Author Manuscript

2001; White and Powell, 2002). Several studies suggest that kinetic factors may inhibit mineral nucleation (i.e., "overstepping"), questioning the applicability of equilibrium thermodynamics to model these type of problems (Carlson et al., 2015; Pattinson et al., 2011; Ridely and Thompson, 1986; Spear and Pattison, 2017). The temperature discrepancy between an equilibrium and non-equilibrium model is often reported to be ~20–50 °C for overstepping the garnet isograd (Castro and Spear, 2017; Spear and Pattison, 2017); this uncertainty is similar to the overall uncertainties associated with the thermodynamic dataset as well as with the parametrization of *a*–*X* relations (Lanari and Duesterhoeft, 2018; Powell and Holland, 2008), and even with those associated with other types of geological uncertainties (Lanari and Engi, 2017; Palin et al., 2016).

In subduction zones, internal and external fluids are likely available during metamorphism and are mobile due to deformation along with the slab–mantle interface, driving mineral reactions; Thus we posit that metamorphism of the subducted oceanic crust, as shown in our models (Figures 5–7) and other studies (e.g., Baxter and Caddick, 2013; Condit et al., 2015; Hacker et al., 2008; Hernández-Uribe and Palin, 2019a; Konrad-Schmolke et al., 2011; van Keken et al., 2011), occur closer to equilibrium conditions. We thus interpret that our results presented herein can reproduce first-order petrological observations that occur in most subduction zones and that mineral overstepping—if any—may not severely modify the observations made here.

CONCLUDING REMARKS

This contribution shows the versatility of applying petrological modeling to HP metabasites to address different geological questions. We demonstrate that the *P*–*T* evolution of the considered examples can be refined and that forward modeling phase assemblages during warm subduction

of the uppermost portion of the oceanic crust can provide unique insights into slab-top dehydration and melting. In particular, we show that:

1. Glaucophane eclogite and garnet−glaucophane schist from the Renge belt (Omi area) experienced peak metamorphism at ~2.0–2.3 GPa and ~550–630 °C. Prograde metamorphism occurred along a d*T*/d*P* gradient of ~71−114 °C/GPa. The post-peak metamorphism occurred at 0.9 GPa and ~500 °C for the glaucophane eclogite and ~1.3 GPa and ~530 °C garnet glaucophane schist.
2. Quartz eclogite from the Sanbagawa belt (Gongen, Besshi area) experienced peak metamorphism at 2.5–2.8 GPa and ~640–750 °C. Prograde metamorphism occurred along a d*T*/d*P* gradient of ~114 °C/GPa. After reaching peak conditions, the quartz eclogite experienced partial melting, observed in the field, and shown in our models. Anatexis at peak conditions likely modified to some extent the original bulk-composition. Early retrogression occurred at ~1.3–1.7 GPa and ~620–690 °C.
3. During subduction along the Nankai *P*–*T* path of fresh and altered oceanic crust, fluid release occurs at ~20–60 km. The main fluid-release pulse is controlled by chlorite breakdown. Our results agree with the location of intermediate-depth earthquakes, indicating that the fluid liberated may produce enough fluid to create elevated pore-fluid pressures promoting seismicity.
4. Our models predict partial melting of the uppermost part of the crust in the warm Nankai subduction zone. According to our models, slab anatexis is not an efficient mechanism for generating voluminous magmatism at the modeled conditions. The calculated melt compositions have adakitic signatures, specifically, the geochemical signatures are

Author Manuscript

similar to those of high-SiO_2 adakites. Notably, the modeled compositions are in good agreement with quaternary adakites from the Daisen and Sambe volcanoes, in SW Japan.

Author Manuscript

ORCID

David Hernández-Uribe: https://orcid.org/0000-0002-5335-4131

Fabián Gutiérrez-Aguilar: https://orcid.org/0000-0003-3644-2567

ACKNOWLEDGMENTS

We thank R. Holder, R. Palin, and C. Yakymchuk for stimulating discussion. The authors have no conflict of interest to declare. Reviews by J. Walters and an anonymous reviewer greatly improved the manuscript and are gratefully acknowledged. T. Tsujimori is thanked for editorial handling.

FIGURE CAPTIONS

Figure 1. Tectonic map of Japan showing the location of the studied areas. The Renge belt and equivalents are shown in purple and the Sanbagawa belt in green (modified from Pastor-Galán et al., 2021). Yellow stars indicate the location of the modeled samples (see text for details). The red star and the black dashed line indicate the location of the subduction zone thermal model of Abers et al. (2013) used in this work (see text for details). NAP–North American Plate; PSP–Philippine Sea Plate; PP–Pacific Plate.

Figure 2. Petrological models for (a–b) glaucophane eclogite and (c–d) garnet glaucophane schist from the Renge belt. (a and c) Pressure-temperature phase diagrams labeled with the stable mineral assemblages. (b and d) Same phase diagram as in (a) and (c) but contoured with mineral

compositional isopleths. The grey fields indicate the peak paragenesis and the stars the prefer peak conditions; the colored-solid lines indicate mineral stability boundaries. Mineral abbreviations follow the guidelines of Whitney and Evans (2010).

Figure 3. Petrological models for quartz eclogite from the Sanbagawa belt (Gongen, Besshi area). (a) Pressure-temperature phase diagrams labeled with the stable mineral assemblages. (b) Same phase diagram as in (a) but contoured with mineral compositional isopleths. The grey fields indicate the peak paragenesis and the stars the prefer peak conditions; the colored-solid lines indicate mineral stability boundaries. Mineral abbreviations follow the guidelines of Whitney and Evans (2010).

Figure 4. Synthesis of *P–T* results for the (a) Renge belt and (b) Sanbagawa belt. The dashed colored boxes represent the observed mineral assemblage fields from Figures 2 and 3; the darker colors represent the *P–T* conditions delimited by modeled isopleths and the stars the preferred peak conditions (the black bars represent the ±1 kbar and ±50 °C uncertainties associated with the technique, see the Methods sections for details). The Renge eclogite *P–T* estimates are from Tsujimori (2002) and the Iratsu eclogites estimates from Endo and Tsuboi (2013), Miyamoto et al. (2007), and Ota et al. (2004). Metamorphic facies diagram modified from Liou et al. (2004). E03–Endo and Tsuboi (2013); EI–Eastern Iratsu (Endo and Tsuboi, 2013); WI–Western Iratsu (Endo and Tsuboi, 2013); O04–Ota et al. (2004); T02–Tsujimori (2002); W15–Weller et al. (2015).

Figure 5. Modeled phase assemblages (only solids + melt) stable along the Nankai subudction geotherm for (a) fresh MORB composition and (b) altered OC. Mineral abbreviations follow the guidelines of Whitney and Evans (2010).

Author Manuscript

Author Manuscript

Figure 6. Modeled melt compositions. (a) MgO vs SiO_2 diagram (Martin et al., 2005) to discriminate between low-SiO_2 adakites (LSA) and high-SiO_2 adakites (HSA). [1]Daisen adakites are from Kimura et al. (2004). (b) Chondrite normalized (McDonough and Sun, 1995) trace-element patterns for melts derived from fresh MORB and altered oceanic crust. [2]The Daisen and Sambe adakites are from Morris (1995). (c) Sr/Y vs Y diagram (Defant and Drummond, 1990) to discriminate adakites from other arc lavas. ADR−Andesite-dacite-rhyolite.

Figure 7. Dehydration during subduction along the Nankai geotherm and its relationship with seismicity. (a) H_2O released (wt. %), (b) H_2O in the solid assemblage (wt. %), and (c) distribution of non-volcanic tremor (modified from Condit et al., 2020). NVT−Non-volcanic tremor.

TABLE CAPTIONS

Table 1. Bulk-rock compositions used for petrological modeling (normalized mol.%).

Table 2. Modeled major (normalized wt. %) and trace-element compositions (μg/g) of modeled melts along the Nankai geotherm.

REFERENCES

Abers, G. A., Nakajima, J., van Keken, P. E., Kita, S., & Hacker, B. R. (2013). Thermal–petrological controls on the location of earthquakes within subducting plates. *Earth and Planetary Science Letters, 369*, 178−187.

Aoki, S., Aoki, K., Chiba, K., Sakata, S., Tsuchiya, Y., & Kato, D. (2020). Origin of the Tonaru body in the Sanbagawa metamorphic belt, SW Japan. *Island Arc, 29*(1), e12332.

Author Manuscript

Aoki, S., Aoki, K., Tsujimori, T., Sakata, S, & Tsuchiya, Y. (2020). Oceanic-arc subduction, stagnation, and exhumation: zircon U–Pb geochronology and trace-element geochemistry of the Sanbagawa eclogites in central Shikoku, SW Japan. *Lithos*, 358–359.

Aoya, M. (2001). *P–T–D* path of eclogite from the Sambagawa belt deduced from combination of petrological and microstructural analyses. *Journal of Petrology, 42*, 1225–1248.

Arakawa, M., Okamoto, K., Yi, K., Terabayashi, M., & Tsutsumi, Y. (2013). SHRIMP U–Pb dating of zircons related to the partial melting in a deep subduction zone: Case study from the S anbagawa quartz-bearing eclogite. *Island Arc*, *22*(1), 74–88.

Banno, S. (1958). Glaucophane schists and associated rocks in the Omi district, Niigata Prefecture, Japan: *Japanese Journal of Geology and Geography, 29*, 29–44.

Banno, S., Sakai, C. (1989). Geology and metamorphic evolution of the Sanbagawa metamorphic belt, Japan. Evolution of Metamorphic Belts, *Geological Society Special Publication, 43*, 519–532.

Baxter, E. F., Caddick, M. J. (2013). Garnet growth as a proxy for progressive subduction zone dehydration. *Geology 41*(6), 643–646.

Baziotis, I., Tsai, C. H., Ernst, W. G., Jahn, B. M., & Iizuka, Y. (2017). New P–T constraints on the Tamayen glaucophane-bearing rocks, eastern Taiwan: Perple_X modelling results and geodynamic implications. *Journal of Metamorphic Geology*, *35*(1), 35–54.

Bédard, J.H. (2006). A catalytic delamination–driven model for coupled genesis of Archaean crust and sub–continental lithospheric mantle. *Geochimica et Cosmochimica Acta, 70*, 1188–1214.

Author Manuscript

Berry, A. J., Stewart, G. A., O'Neill, H. S. C., Mallmann, G., & Mosselmans, J. F. W. (2018). A re–assessment of the oxidation state of iron in MORB glasses. *Earth and Planetary Science Letters 483*, 114–123.

Caddick, M. J., Konopásek, J., & Thompson, A. B. (2010). Preservation of garnet growth zoning and the duration of prograde metamorphism. *Journal of Petrology*, *51*(11), 2327–2347.

Cao, W., Gilotti, J. A., Massonne, H. J., Ferrando, S., & Foster Jr, C. T. (2019). Partial melting due to breakdown of an epidote-group mineral during exhumation of ultrahigh- pressure eclogite: An example from the North-East Greenland Caledonides. *Journal of Metamorphic Geology*, *37*(1), 15–39.

Carlson, W. D., Pattison, D. R. M., & Caddick, M. J. (2015). Beyond the equilibrium paradigm: How consideration of kinetics enhances metamorphic interpretation. *American Mineralogist*, *100*(8–9), 1659–1667.

Carswell, D. A., O'Brien, P. J., Wilson, R. N., & Zhai, M. (1997). Thermobarometry of phengite-bearing eclogites in the Dabie Mountains of central China. *Journal of Metamorphic Geology, 15*(2), 239–252.

Castro, A. E., Spear, F. S. (2017). Reaction overstepping and re–evaluation of peak P–T conditions of the blueschist unit Sifnos, Greece: implications for the Cyclades subduction zone. *International Geology Review, 59*(5–6), 548–562.

Condit, C. B., Guevara, V. E., Delph, J. R., & French, M. E. (2020). Slab dehydration in warm subduction zones at depths of episodic slip and tremor. *Earth and Planetary Science Letters, 552*, 116601.

Author Manuscript

de Capitani, C., & Brown, T. H. (1987). The computation of chemical equilibrium in complex systems containing non–ideal solutions. *Geochimica et Cosmochimica Acta 51*(10), 2639–2652.

de Capitani, C., & Petrakakis, K. (2010). The computation of equilibrium assemblage diagrams with Theriak/Domino software. *American Mineralogist 95*(7), 1006–1016.

Defant, M. J., and Drummond, M. S. (1990). Derivation of some modern arc magmas by melting of young subducted lithosphere. *Nature, 347*(6294), 662.

Diener, J. F. A., Powell, R. (2010). Influence of ferric iron on the stability of mineral assemblages. *Journal of Metamorphic Geology, 28*(6), 599–613.

Dragovic, B., Angiboust, S., & Tappa, M. J. (2020). Petrochronological close–up on the thermal structure of a paleo–subduction zone (W. Alps). *Earth and Planetary Science Letters, 547*, 116446.

Enami, M., Kimura, J. I., Tsuboi, M., Kouketsu, Y., Nagaya, T., & Huang, S. (2019). Coexisting different types of zoned garnet in kyanite-quartz eclogites from the Sanbagawa metamorphic belt: Evidence of deformation-induced lithological mixing during prograde metamorphism. *Island Arc*, *28*(1), e12274.

Enami, M., Mizukami, T., & Yokoyama, K. (2004). Metamorphic evolution of garnet-bearing ultramafic rocks from the Gongen area, Sanbagawa belt, Japan. *Journal of Metamorphic Geology, 22*(1), 1–15.

Endo, S., Tsuboi, M., (2013). Petrogenesis and implications of jadeite–bearing kyanite eclogite from the Sanbagawa belt (SW Japan). *Journal of Metamorphic Geology, 31*, 647–661.

Endo, S., Wallis, S. R., Tsuboi, M., Aoya, M., & Uehara, S. I. (2012). Slow subduction and buoyant exhumation of the Sanbagawa eclogite. *Lithos, 146*, 183–201.

Author Manuscript

Evans, B. W. (1990). Phase relations of epidote–blueschists: *Lithos*, *25*, 3–23.

Fagereng, A., Diener, J.F.A., Meneghini, F., Harris, C., Kvadsheim, A. (2018). Quartz vein formation by local dehydration embrittlement along the deep, tremorgenic sub-duction thrust interface. *Geology, 46*, 67–70.

Gale, A., Dalton, C. A., Langmuir, C. H., Su, Y., & Schilling, J. G. (2013). The mean composition of ocean ridge basalts. *Geochemistry, Geophysics, Geosystems 14*(3), 489–518.

Green, E. C. R., White, R. W., Diener, J. F. A., Powell, R., Holland, T. J. B., & Palin, R. M. (2016). Activity–composition relations for the calculation of partial melting equilibria in metabasic rocks. *Journal of Metamorphic Geology 34*(9), 845–869.

Groppo, C., Rolfo, F., Liu, Y. C., Deng, L. P., & Wang, A. D. (2015). PT evolution of elusive UHP eclogites from the Luotian dome (North Dabie Zone, China): How far can the thermodynamic modeling lead us? *Lithos*, *226*, 183–200.

Guevara, V. E., Caddick, M. J. (2016). Shooting at a moving target: phase equilibria modelling of high–temperature metamorphism. *Journal of Metamorphic Geology*, *34*(3), 209–235.

Guevara, V. E., Caddick, M. J., & Dragovic, B. (2017). Rapid high-T decompressi on recorded by Archean granulites in the northern Wyoming Province: Insights from petrological modelling. *Journal of Metamorphic Geology*, *35*(9), 943–965.

Guiraud, M., Powell, R., & Rebay, G. (2001). H_2O in metamorphism and unexpected behaviour in the preservation of metamorphic mineral assemblages. *Journal of Metamorphic Geology*, *19*(4), 445–454.

Gutiérrez-Aguilar, F., Schaaf, P., Solís-Pichardo, G., Arrieta-García, G. F., Hernández-Treviño, T., & Linares-López, C. (2021). Phase equilibrium modelling of the amphibolite facies

Author Manuscript

metamorphism in the Yelapa–Chimo Metamorphic Complex, Mexico. *Geoscience Frontiers, 12*(1), 293–312.

Hacker, B. R. (2006). Pressures and temperatures of ultrahigh–pressure metamorphism: implications for UHP tectonics and H_2O in subducting slabs. *International Geology Review*, *48*(12), 1053–1066.

Hacker, B. R. (2008). H_2O subduction beyond arcs. *Geochemistry, Geophysics, Geosystems, 9*(3).

Hattori, K., Wallis, S., Enami, M. & Mizukami, T. (2010). Subduction of mantle wedge peridotites: evidence from the Higashi–akaishi ultramafic body in the Sanbagawa metamorphic belt. *Island Arc, 19,* 192–207.

Hensen, B.J. (1971). Theoretical phase relations involving cordierite and garnet in the system $MgO–FeO–Al_2O_3–SiO_2$: *Contributions to Mineralogy and Petrology*, *33,* 191–214.

Hernández-Montenegro, J. D., Palin, R. M., Zuluaga, C. A., & Hernández-Uribe, D. (2021). Archean continental crust formed by magma hybridization and voluminous partial melting. Scientific Reports, 11(1), 1–9.

Hernández-Uribe, D., & Palin, R. M. (2019b). Catastrophic shear–removal of subcontinental lithospheric mantle beneath the Colorado Plateau by the subducted Farallon slab. *Scientific reports*, *9*(1), 1–10.

Hernández-Uribe, D., Gutiérrez-Aguilar, F., Mattinson, C. G., Palin, R. M., & Neill, O. K. (2019). A new record of deeper and colder subduction in the Acatlán complex, Mexico: Evidence from phase equilibrium modelling and Zr–in–rutile thermometry. *Lithos, 324*, 551–568.

Author Manuscript

Hernández-Uribe, D., Hernández-Montenegro, J. D., Cone, K. A., & Palin, R. M. (2020). Oceanic slab–top melting during subduction: Implications for trace–element recycling and adakite petrogenesis. *Geology, 48*(3), 216–220.

Hernández-Uribe, D., Palin, R. M., Cone, K. A., & Cao, W. (2020). Petrological implications of seafloor hydrothermal alteration of subducted mid–ocean ridge basalt. *Journal of Petrology*.

Hernández-Uribe, D., Mattinson, C. G., & Zhang, J. (2018). Phase equilibrium modelling and implications for P–T determinations of medium-temperature UHP eclogites, Nor th Qaidam terrane, China. *Journal of Metamorphic Geology, 36*(9), 1237–1261.

Hernández-Uribe, D., Palin, R. M. (2019a) A revised petrological model for subducted oceanic crust: insights from phase equilibria modeling. *Journal of Metamorphic Geology 37*(6), 745–768.

Holland, T. J. B., Powell, R. (1998). An internally consistent thermodynamic data set for phases of petrological interest. *Journal of Metamorphic Geology, 16*(3), 309–343.

Holland, T. J. B., Powell, R. (2001). Calculation of phase relations involving haplogranitic melts using an internally consistent thermodynamic dataset. *Journal of Petrology*, *42*(4), 673–683.

Holland, T. J. B., Powell, R. (2003). Activity–composition relations for phases in petrological calculations: an asymmetric multicomponent formulation. *Contributions to Mineralogy and Petrology*, *145*(4), 492–501.

Holland, T. J. B., Powell, R. (2011). An improved and extended internally consistent thermodynamic dataset for phases of petrological interest, involving a new equation of state for solids. *Journal of Metamorphic Geology, 29*(3), 333–383.

Author Manuscript

Hyndman, R.D., Mccrory, P.A., Wech, A., Kao, H., Ague, J. (2015). Cascadia subduct-ing plate fluids channelled to fore-arc mantle corner: ETS and silica depo-sition. *Journal of Geophysical Research Solid Earth 120*, 4344–4358.

Itaya, T., Tsujimori, T., & Liou, J. G. (2011). Evolution of the Sanbagawa and Shimanto high–pressure belts in SW Japan: Insights from K–Ar (Ar–Ar) geochronology. *Journal of Asian Earth Sciences*, *42*(6), 1075–1090.

Kendrick, J., Yakymchuk, C. (2020). Garnet fractionation, progressive melt loss and bulk composition variations in anatectic metabasites: complications for interpreting the geodynamic significance of TTGs. *Geoscience Frontiers, 11*(3), 745–763.

Kimura, J. I., Gill, J. B., Kunikiyo, T., Osaka, I., Shimoshioiri, Y., Katakuse, M., ... & Stern, R. J. (2014). Diverse magmatic effects of subducting a hot slab in SW Japan: Results from forward modeling. *Geochemistry, Geophysics, Geosystems*, *15*(3), 691–739.

Kimura, J. I., Stern, R. J., & Yoshida, T. (2005). Reinitiation of subduction and magmatic responses in SW Japan during Neogene time. *Geological Society of America Bulletin, 117*(7–8), 969–986.

Klonowska, I., Janák, M., Majka, J., Petrik, I., Froitzheim, N., Gee, D. G., & Sasinková, V. (2017). Microdiamond on Åreskutan confirms regional UHP metamorphism in the Seve Nappe Complex of the Scandinavian Caledonides. *Journal of Metamorphic Geology, 35*(5), 541–564.

Konrad–Schmolke, M., Handy, M. R., Babist, J., & O'Brien, P. J. (2005). Thermodynamic modelling of diffusion–controlled garnet growth. *Contributions to Mineralogy and Petrology, 149*(2), 181–195.

Author Manuscript

Konrad–Schmolke, M., O'Brien, P. J., & Zack, T. (2011). Fluid migration above a subducted slab—constraints on amount, pathways and major element mobility from partially overprinted eclogite–facies rocks (Sesia Zone, Western Alps). *Journal of Petrology, 52*(3), 457–486.

Krogh, E. J., 1988, The garnet–clinopyroxene Fe–Mg geothermometer—a reinterpretation of existing experimental data: *Contributions to Mineralogy and Petrology, 75,* 387–393.

Kunugiza, K., Goto, A., Itaya, T. and Yokoyama, K. (2004) Geological development of the Hida Gaien belt: constraints from K–Ar ages of high P/T metamorphic rocks and U–Th–Pb EMP ages of granitic rocks affecting contact metamorphism of serpentinite. *Journal of Geological Society of Japan, 110,* 580–590 (Japanese with English abstract).

Kunugiza, K., Nakamura, E., Goto, A., Kobayashi, K., Ota, T., Miyajima, H., & Yokoyama, K. (2017). In–situ U–Pb zircon age dating deciphering the formation event of the omphacite growth over relict edenitic pargasite in omphacite–bearing jadeitite of the Itoigawa–Omi area of the Hida–Gaien belt, central Japan. *Journal of Mineralogical and Petrological Sciences, 112*(5), 256–270.

Lanari, P., Duesterhoeft, E. (2019). Modeling metamorphic rocks using equilibrium thermodynamics and internally consistent databases: past achievements, problems and perspectives. *Journal of Petrology 60*(1), 19–56.

Lanari, P., Engi, M. (2017). Local bulk composition effects on metamorphic mineral assemblages. *Reviews in Mineralogy and Geochemistry, 83*(1), 55–102.

Lanari, P., Ferrero, S., Goncalves, P., & Grosch, E. G. (2019). Metamorphic geology: progress and perspectives. *Geological Society, London, Special Publications, 478*(1), 1–12.

Author Manuscript

Li, S. S., Palin, R. M., Santosh, M., Shaji, E., & Tsunogae, T. (2020). Extreme thermal metamorphism associated with Gondwana assembly: Evidence from sapphirine–bearing granulites of Rajapalayam, southern India. *GSA Bulletin, 132*(5–6), 1013–1030.

Liou, J. G., Tsujimori, T., Zhang, R. Y., Katayama, I., & Maruyama, S. (2004). Global UHP metamorphism and continental subduction/collision: the Himalayan model. *International Geology Review, 46*(1), 1–27.

Martin, H., Smithies, R. H., Rapp, R., Moyen, J. F., and Champion, D. (2005). An overview of adakite, tonalite–trondhjemite–granodiorite (TTG), and sanukitoid: relationships and some implications for crustal evolution. *Lithos, 79*(1–2), 1–24.

Massonne, H. J. (2012). Formation of amphibole and clinozoisite–epidote in eclogite owing to fluid infiltration during exhumation in a subduction channel. *Journal of Petrology, 53*(10), 1969–1998.

Massonne, H. J. (2015). Derivation of P–T paths from high–pressure metagranites—Examples from the Gran Paradiso Massif, western Alps. *Lithos, 226*, 265–279.

Matsumoto, M., Wallis, S., Aoya, M., Enami, M., Kawano, J., Seto, Y. and Shimobayashi, N. (2003) Petrological constraints on the formation conditions and retrograde P–T path of the Kotsu eclogite unit, central Shikoku. *Journal of Metamorphic Geology, 21*, 363–376.

McDonough, W. F., Sun, S. S. (1995). The composition of the Earth. *Chemical Geology, 120*(3–4), 223–253.

Miyagi, Y., Takasu, A. (2005). Prograde eclogites from the Tonaru epidote amphibolite mass in the Sambagawa Metamorphic Belt, central Shikoku, southwest Japan. *Island Arc, 14*(3), 215–235.

Author Manuscript

Miyamoto, A., Enami, M., Tsuboi, M., & Yokoyama, K. (2007). Peak conditions of kyanite–bearing quartz eclogites in the Sanbagawa metamorphic belt, central Shikoku, Japan. *Journal of Mineralogical and Petrological Sciences, 102*(6), 352–367.

Miyashiro, A., 1961. Evolution of metamorphic belts. *Journal of Petrology, 2*, 277–311.

Morris, P. A. (1995). Slab melting as an explanation of Quaternary volcanism and aseismicity in southwest Japan SW Japan. *Geology, 23*(5), 395–398.

Moyen, J. F. (2009). High Sr/Y and La/Yb ratios: the meaning of the "adakitic signature". *Lithos, 112*(3–4), 556–574.

Ota, T., Terabayashi, M., & Katayama, I. (2004). Thermobaric structure and metamorphic evolution of the Iratsu eclogite body in the Sanbagawa belt, central Shikoku, Japan. *Lithos, 73*(1–2), 95–126.

Palin, R. M., Searle, M. P., Waters, D. J., Horstwood, M. S. A., & Parrish, R. R. (2012). Combined thermobarometry and geochronology of peraluminous metapelites from the Karakoram metamorphic complex, North Pakistan; New insight into the tectonothermal evolution of the Baltoro and Hunza Valley regions. J*ournal of Metamorphic Geology, 30*(8), 793–820.

Palin, R. M., Weller, O. M., Waters, D. J., & Dyck, B. (2016). Quantifying geological uncertainty in metamorphic phase equilibria modelling; a Monte Carlo assessment and implications for tectonic interpretations. *Geoscience Frontiers, 7*(4), 591–607.

Palin, R.M., White, R.W. & Green, E.C. (2016). Partial melting of metabasic rocks and the generation of tonalitic–trondhjemitic–granodioritic (TTG) crust in the Archaean: Constraints from phase equilibrium modelling. *Precambrian Research, 287*,73–90.

Author Manuscript

Pastor-Galán, D., Spencer, C. J., Furukawa, T., & Tsujimori, T. (2021). Evidence for crustal removal, tectonic erosion and flare-ups from the Japanese evolving forearc sediment. *Earth and Planetary Science Letters*, 564, 116893.

Pattison, D. R. M., Chacko, T., Farquhar, J., and McFarlane, C. R. M. (2003)/ Temperatures of granulite–facies metamorphism: Constraints from experimental phase equilibria and thermobarometry corrected for retrograde exchange: *Journal of Petrology, 44*, 867–900.

Pattison, D. R., de Capitani, C., & Gaidies, F. (2011). Petrological consequences of variations in metamorphic reaction affinity. *Journal of Metamorphic Geology, 29*(9), 953–977.

Peacock, S.M., 2009. Thermal and metamorphic environment of subduction zone episodic tremor and slip. *Journal of Geophysical Research, Solid Earth, 114*, 1–9.

Powell, R., (1978). *Equilibrium Thermodynamics in Petrology, An Introduction*. Harper & Row Ltd, London, 284.

Powell, R. (1985). Geothermometry and geobarometry: a discussion. *Journal of the Geological Society, 142*(1), 29-38.

Powell, R., Guiraud, M., & White, R. W. (2005). Truth and beauty in metamorphic phase–equilibria: conjugate variables and phase diagrams. *The Canadian Mineralogist*, *43*(1), 21–33.

Powell, R., Holland, T. J. B. (2008). On thermobarometry. *Journal of Metamorphic Geology*, *26*(2), 155–179.

Powell, R., Holland, T. J. B., & Worley, B. A. (1998). Calculating phase diagrams involving solid solutions via non-linear equations, with exam ples using THERMOCALC. *Journal of metamorphic Geology*, *16*(4), 577–588.

Author Manuscript

Powell, R., Holland, T. J.B. (2010). Using equilibrium thermodynamics to understand metamorphism and metamorphic rocks. *Elements, 6*(5), 309–314.

Proyer, A., Dachs, E., & McCammon, C. (2004). Pitfalls in geothermobarometry of eclogites: Fe3+ and changes in the mineral chemistry of omphacite at ultrahigh pressures: *Contributions to Mineralogy and Petrology*, *147*, 305–318.

Ravna, E. J. K. (2003). Thermobarometric methodologies applicable to eclogites and garnet ultrabasites: *EMU Notes in Mineralogy*, *5*, 229–259.

Rebay, G., Powell, R., & Diener, J. F. A. (2010). Calculated phase equilibria for a MORB composition in a *P–T* range, 450–650 C and 18–28 kbar: the stability of eclogite. *Journal of Metamorphic Geology*, *28*(6), 635–645.

Ridley, J., Thompson, A.B. (1986). The role of mineral kinetics in the development of metamorphic microtextures. In: Walther, J.V., Wood, B.J. (Eds.), Fluid–Rock Inter–actions During Metamorphism. Springer, New York, pp.80–97.

Rosenberg, C.L., Handy, M.R. (2005). Experimental deformation of partially melted granite revisited: Implications for the continental crust. *Journal of Metamorphic Geology, 23*, 19–28.

Rushmer, T. (1995). An experimental deformation study of partially molten amphibolite: Application to low-melt fraction segregation. J*ournal of Geophysical Research: Solid Earth, 100*(B8), 15681–15695.

Shaw, D.M. (2006). Trace elements in magmas: a theoretical treatment. Cambridge University Press.

Author Manuscript

Shinji, Y., Tsujimori, T. (2019). Retrograde pumpellyite in the Yunotani garnet blueschist of the Omi area, Japan: An update on the cooling path. *Journal of Mineralogical and Petrological Sciences*, 180716.

Spear, F. S., Pattison, D. R. (2017). The implications of overstepping for metamorphic assemblage diagrams (MADs). *Chemical Geology*, *457*, 38–46.

Spear, F. S., Pattison, D. R., & Cheney, J. T. (2017). The metamorphosis of metamorphic petrology. The Web of Geological Sciences: Advances, Impacts, and Interactions II. In*: Geological Society of America 523*, 31–73.

Spear, F.S. (1988). The Gibbs method and Duhem's theorem: The quantitative relationships among P, T, chemical potential, phase composition and reaction progress in igneous and metamorphic systems: *Contributions to Mineralogy and Petrology,99*, 249–256,

Spear, F.S. (1995). *Metamorphic phase equilibria and Pressure–Temperature–Time paths*: Mineralogical Society of America, Washington, DC, 799 p.

St–Onge, M. R., Rayner, N., Palin, R. M., Searle, M. P., & Waters, D. J. (2013). Integrated pressure–temperature–time constraints for the Tso Morari dome (Northwest India): implications for the burial and exhumation path of UHP units in the western Himalaya. *Journal of Metamorphic Geology*, *31*(5), 469–504.

Staudigel, H., Davies, G. R., Hart, S. R., Marchant, K. M., & Smith, B. M. (1995). Large scale isotopic Sr, Nd and O isotopic anatomy of altered oceanic crust: DSDP/ODP sites417/418. *Earth and Planetary Science Letters*, *130*(1–4), 169–185.

Štípská, P., & Powell, R. (2005). Constraining the P–T path of a MORB-type eclogite using pseudosections, garnet zoning and garnet-clinopyroxene thermometry: an example from the Bohemian Massif. *Journal of Metamorphic Geology*, *23*(8), 725–743.

Author Manuscript

Tatsumi, Y., Suenaga, N., Yoshioka, S., Kaneko, K., & Matsumoto, T. (2020). Contrasting volcano spacing along SW Japan arc caused by difference in age of subducting lithosphere. *Scientific Reports, 10*(1), 1–11.

Tsujimori, T. (2002). Prograde and retrograde PT paths of the late Paleozoic glaucophane eclogite from the Renge metamorphic belt, Hida Mountains, southwestern Japan. *International Geology Review, 44*(9), 797–818.

Tsujimori, T., & Itaya, T. (1999). Blueschist-facies metamorphism during Paleozoic orogeny in southwestern Japan: Phengite K-Ar ages of blueschist-facies tectonic blocks in a serpentinite melange beneath early Paleozoic Oeyama ophiolite. *The Island Arc, 8*(2), 190–205.

Tsujimori, T., Harlow, G. E. (2017). Jadeitite (jadeite jade) from Japan: History, characteristics, and perspectives. *Journal of Mineralogical and Petrological Sciences, 112*(5), 184–196.

Tsujimori, T., Matsumoto, K. (2006) P–T pseudosection of a glaucophane–epidote eclogite from Omi serpentinite melange, SW Japan: A preliminary report. *Journal of the Geological Society of Japan, 112*, 407–414 (Japanese with English abstract).

van Keken, P. E., Hacker, B. R., Syracuse, E. M., & Abers, G. A. (2011). Subduction factory: 4. Depth-dependent f lux of H_2O from subducting slabs worldwide. *Journal of Geophysical Research: Solid Earth, 116*(B1).

Vigneresse, J. L., Barbey, P., and Cuney, M. (1996). Rheological transitions during partial melting and crystallization with application to felsic magma segregation and transfer. *Journal of Petrology, 37*(6), 1579–1600.

Wallis, S. R., Anczkiewicz, R., Endo, S., Aoya, M., Platt, J. P., Thirlwall, M., & Hirata, T. (2009). Plate movements, ductile deformation and geochronology of the Sanbagawa belt,

Author Manuscript

SW Japan: tectonic significance of 89–88 Ma Lu–Hf eclogite ages. *Journal of Metamorphic Geology, 27*(2), 93–105.

Walters, J. B., Cruz-Uribe, A. M., & Marschall, H. R. (2020). Sulfur loss from subducted altered oceanic crust and implications for mantle oxidation. *Geochemical Perspectives Letters, 13*, 36–41.

Wei, C. J., Clarke, G. L. (2011). Calculated phase equilibria for MORB compositions: a reappraisal of the metamorphic evolution of lawsonite eclogite. *Journal of Metamorphic Geology*, *29*(9), 939–952.

Wei, C. J., Duan, Z. Z. (2019). Phase relations in metabasic rocks: constraints from the results of experiments, phase modelling and ACF analysis. *Geological Society, London, Special Publications, 474*(1), 25–45.

Wei, C. J., Qian, J. H., & Tian, Z. L. (2013). Metamorphic evolution of medium-temperature ultra-high pressure (MT- UHP) eclogites from the South Dabie orogen, Central China: An insight from phase equilibria modelling. *Journal of Metamorphic Geology, 31*(7), 755–774.

Weller, O. M., Wallis, S. R., Aoya, M., & Nagaya, T. (2015). Phase equilibria modelling of blueschist and eclogite from the Sanbagawa metamorphic belt of southwest JapanSW Japan reveals along-strike consistency in tectonothermal architecture. *Journal of Metamorphic Geology, 33*(6), 579–596.

White, R. W., Powell, R., Holland, T. J. B. & Worley, B. A. (2000). The effect of TiO_2 and Fe_2O_3 on metapelitic assemblages at greenschist and amphibolite facies conditions: mineral equilibria calculations in the system K_2O–FeO–MgO–Al_2O_3–SiO_2–H_2O–TiO_2–Fe_2O_3. *Journal of Metamorphic Geology, 18,* 497–511.

White, R. W., Powell, R., Holland, T. J. B., Johnson, T. E., & Green, E. C. R. (2014). New mineral activity–composition relations for thermodynamic calculations in metapelitic systems. *Journal of Metamorphic Geology, 32*(3), 261–286.

White, R.W., Powell, R. & Clarke, G.L. (2002). The interpretation of reaction textures in Fe-rich metapelitic granulites of the Musgrave Block, central Australia: constraints from mineral equilibria calculations in the system K_2O–FeO–MgO–Al_2O_3–SiO_2–H_2O–TiO_2–Fe_2O_3. *Journal of Metamorphic Geology, 20*, 41–55.

Whitney, D. L., & Evans, B. W. (2010). Abbreviations for names of rock–forming minerals. *American Mineralogist, 95*(1), 185–187.

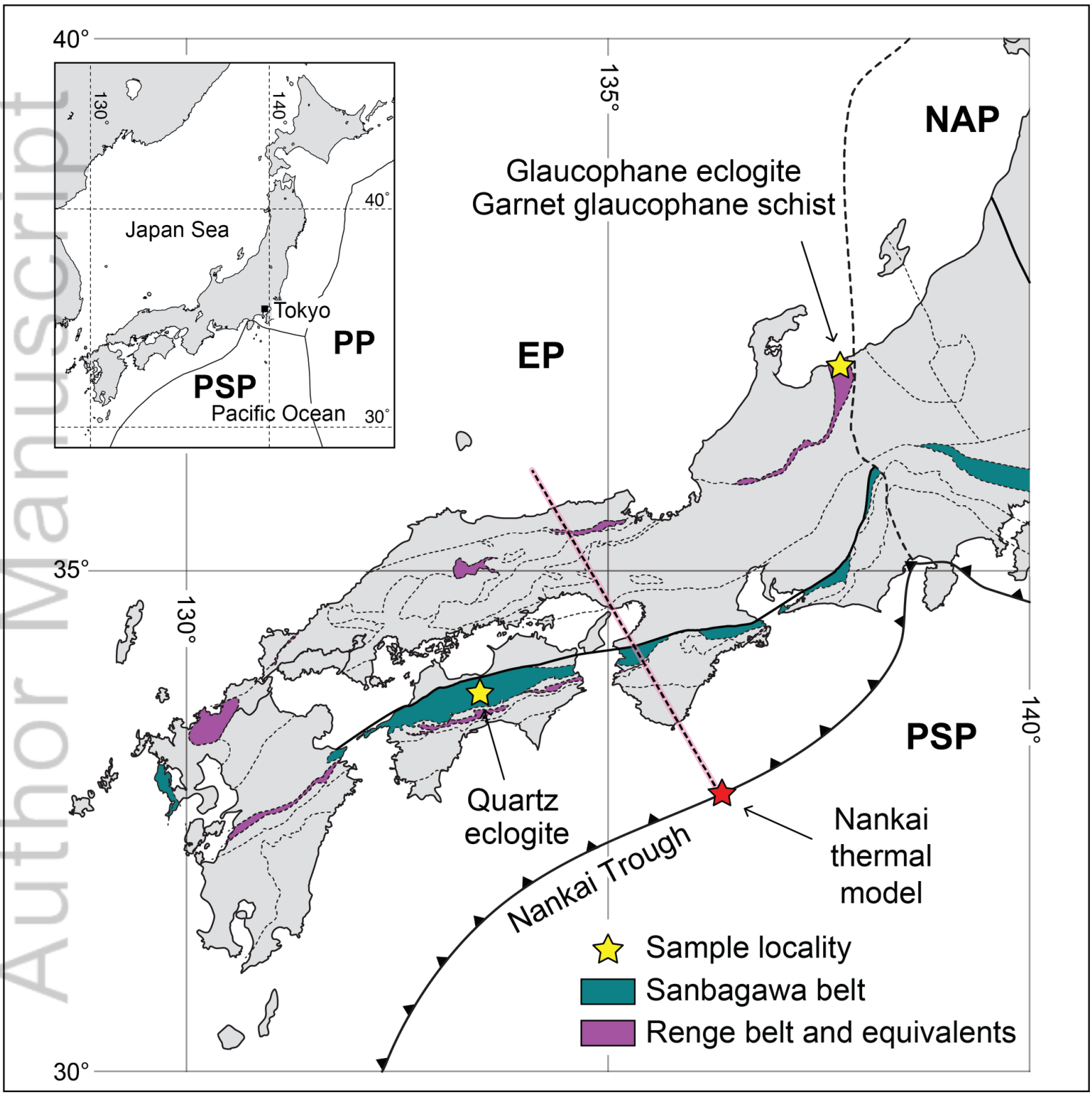
Yakymchuk, C. (2017). Applying phase equilibria modelling to metamorphic and geological processes: recent developments and future potential. *Geoscience Canada, 44*(1), 27–45.

Yamada, C., Tsujimori, T., Chang, Q., & Kimura, J. I. (2019). Boron isotope compositions of antigorite–grade serpentinites in the Itoigawa–Omi area of the Hida–Gaien Belt, Japan. *Journal of Mineralogical and Petrological Sciences, 114*(6), 290–295.

Yoshida, T., Taguchi, T., Ueda, H., Horie, K., & Satish-Kumar, M. (2021). Early Carboniferous HP metamorphism in the Hida Gaien Belt, Japan: Implications for the Palaeozoic tectonic history of proto-Japan. *Journal of Metamorphic Geology, 39*, 77–100

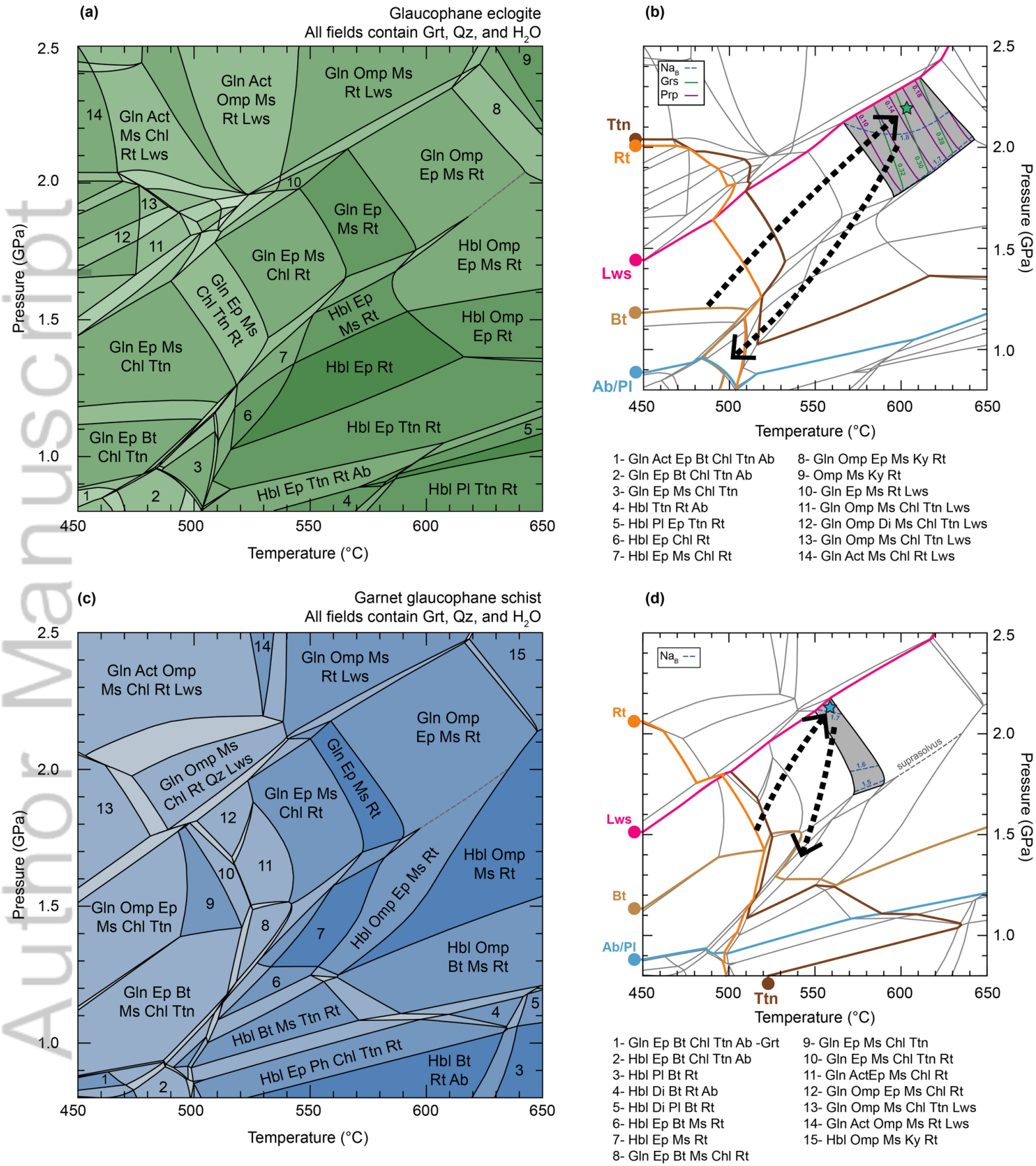
Zellmer, G. F., Iizuka, Y., Miyoshi, M., Tamura, Y., & Tatsumi, Y. (2012). Lower crustal H_2O controls on the formation of adakitic melts. *Geology, 40*(6), 487–490.

Author Manuscript



Author Manuscript

IAR_12406_Fig. 1.png



Author Manuscript

Figure 2

IAR_12406_Fig. 2.png

Author Manuscript

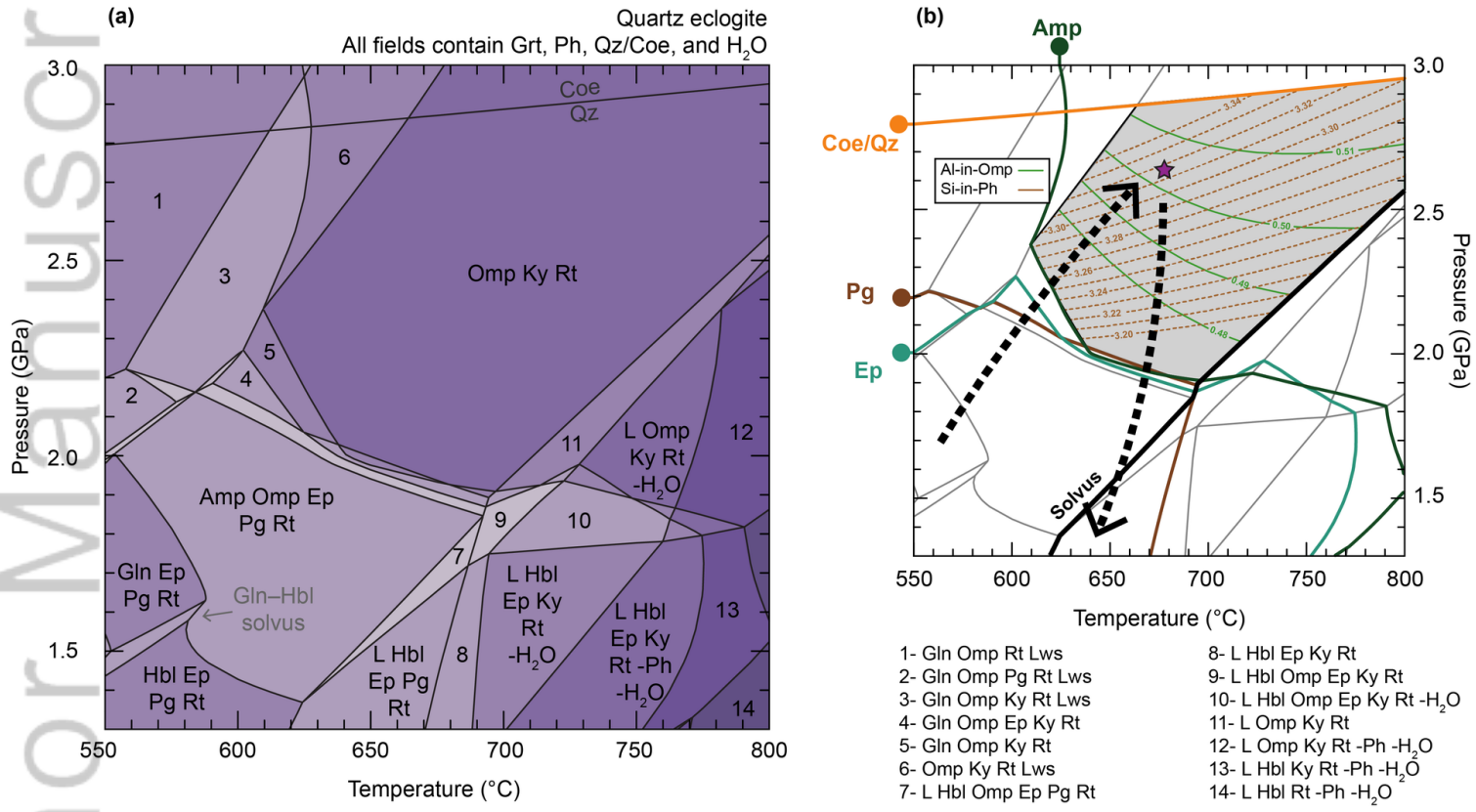


Figure 3

IAR_12406_Fig. 3.png

Author Manuscript

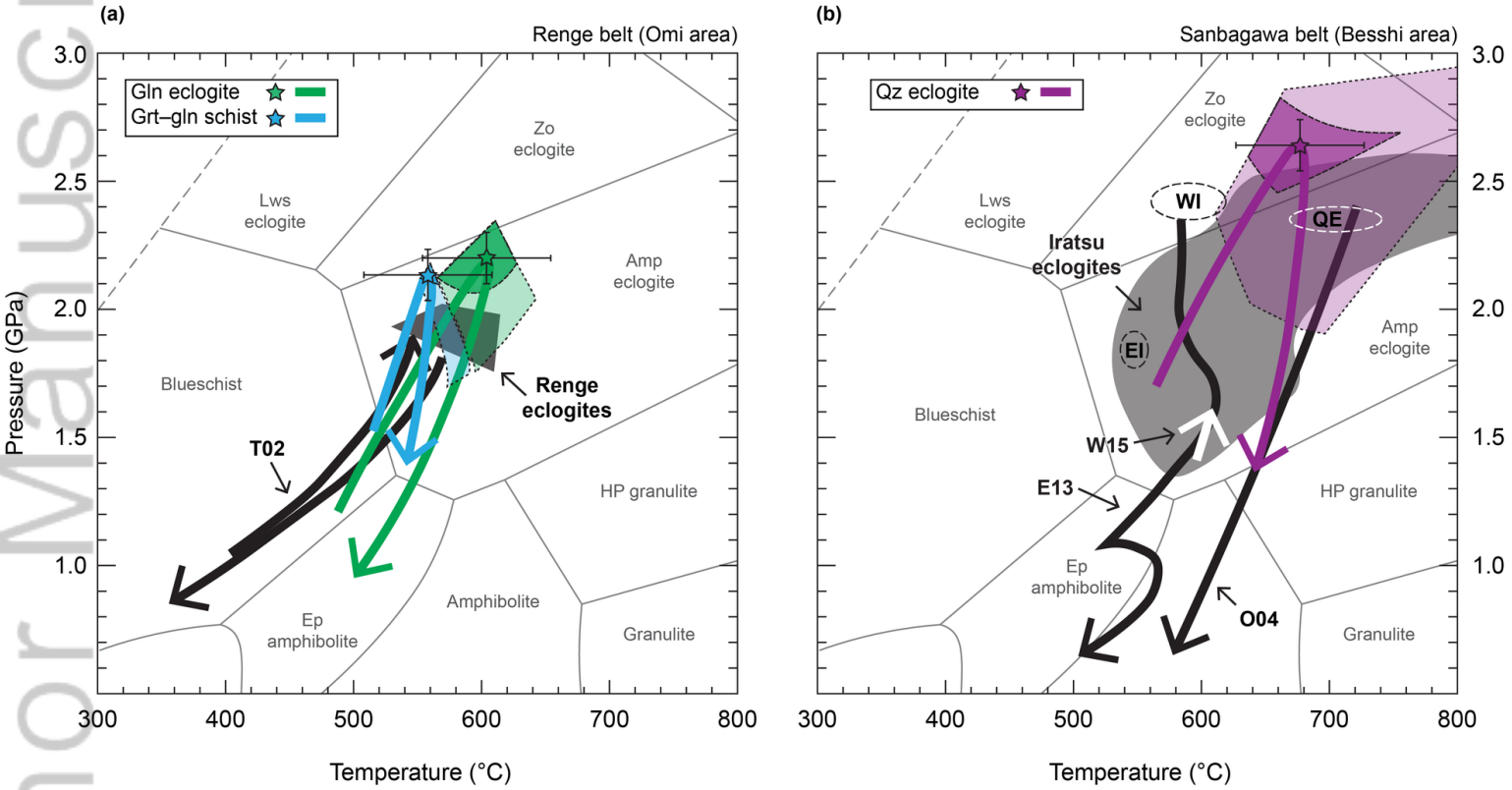


Figure 4

IAR_12406_Fig. 4.png

Author Manuscript

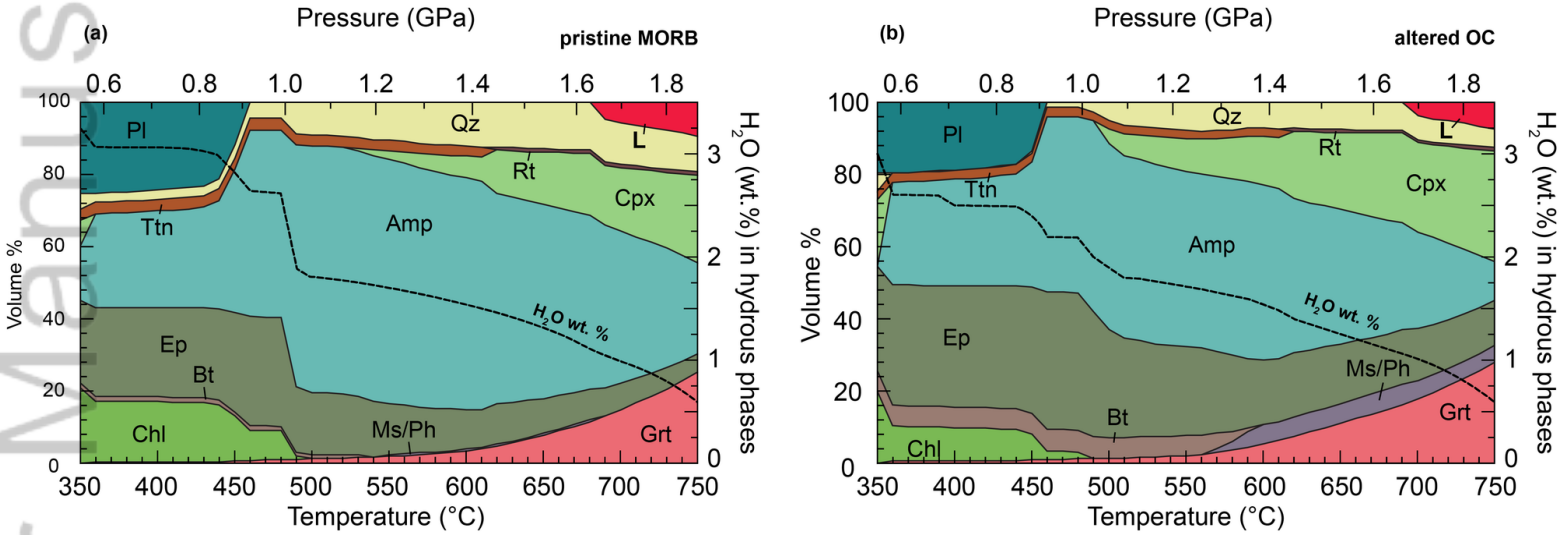


Figure 5

IAR_12406_Fig. 5.png

Author Manuscript

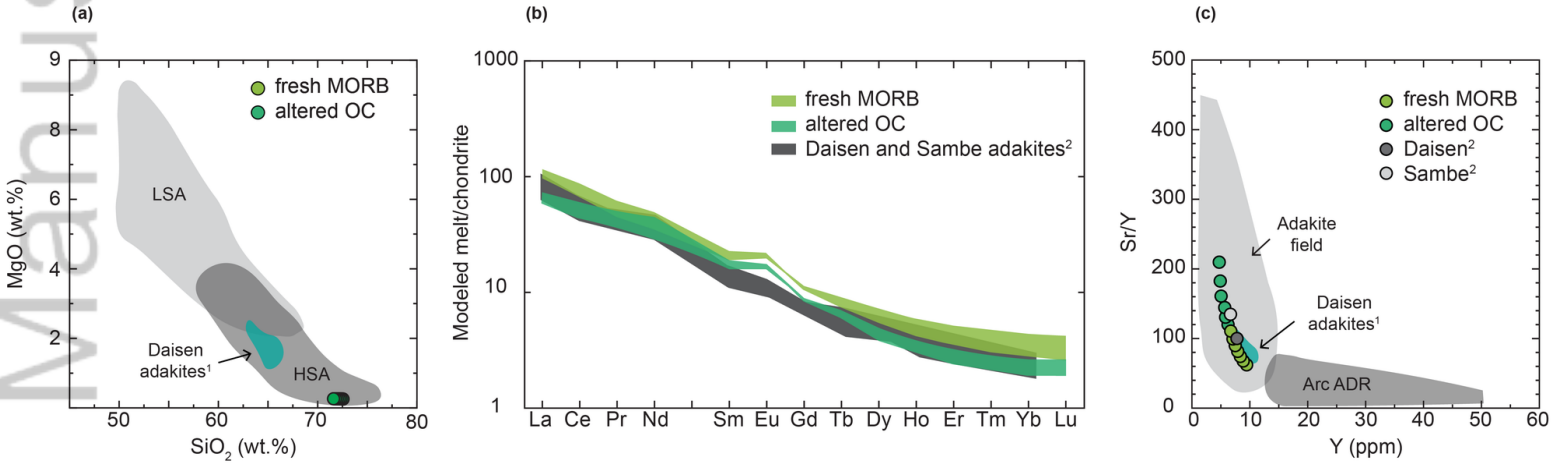


Figure 6

IAR_12406_Fig. 6.png

Author Manuscript

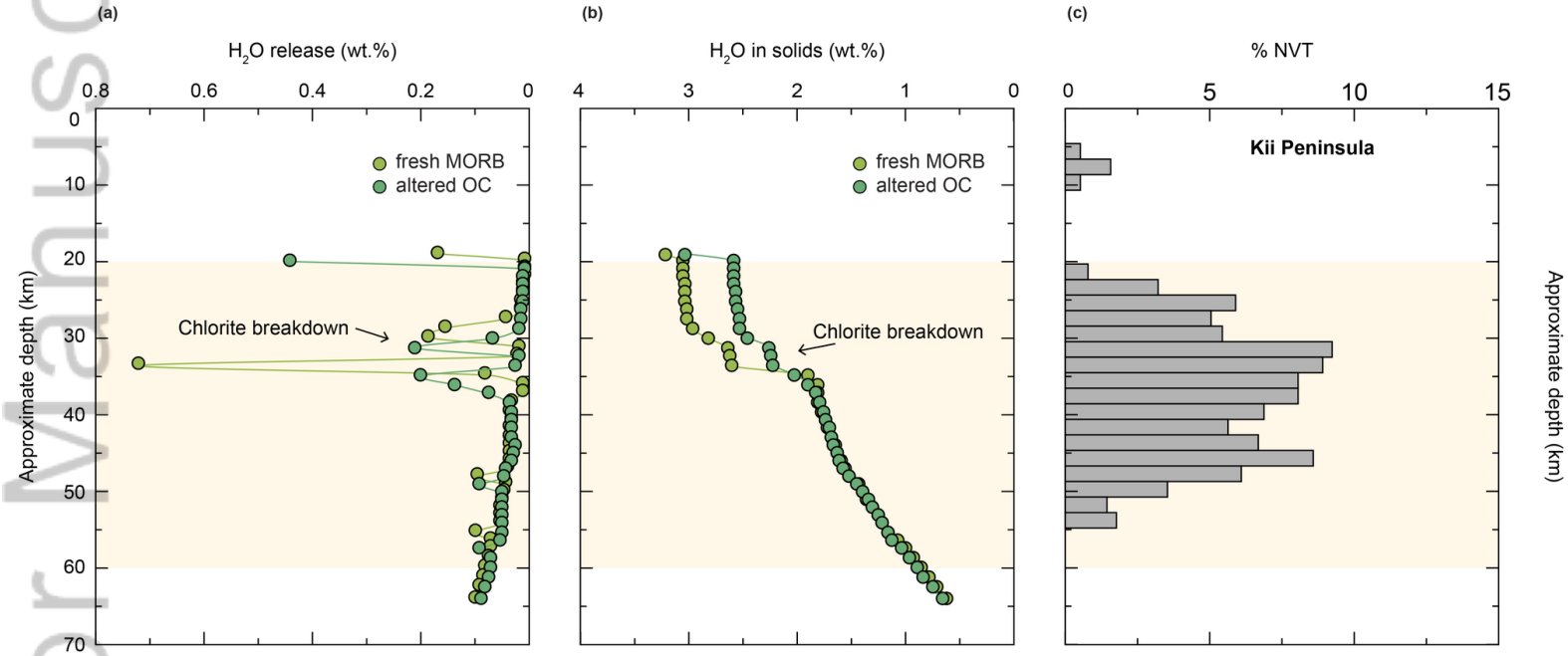


Figure 7

IAR_12406_Fig. 7.png

Table 1. Bulk-rock compositions used for petrological modeling (normalized mol.%).

Sample	Figs	H_2O	SiO_2	Al_2O_3	CaO	MgO	FeO^{tot}	K_2O	Na_2O	TiO_2	MnO	O	X_{Mg}
Glaucophane eclogite	2a,b	excess	53.94	9.79	10.13	10.05	10.64	0.03	2.88	1.32	0.16	1.06	0.49
Garnet glaucophane schist	2b,c	excess	52.69	8.58	7.68	13.06	10.81	0.58	3.54	1.29	0.13	1.62	0.55
Quartz eclogite	4a,b	excess	73.12	8.07	4.74	4.12	6.20	0.47	2.16	0.38	0.12	0.62	0.40
MORB	5a	excess	52.44	9.27	12.41	12.03	8.53	0.09	2.85	1.20	0.15	1.02	0.59
MORB	5a	5.62	49.49	8.75	11.71	11.35	8.05	0.09	2.69	1.13	0.14	0.97	0.59
altered OC	5b	excess	50.68	10.13	15.10	10.98	8.35	0.40	2.22	0.98	0.17	1.00	0.57
altered OC	5b	5.02	48.14	9.62	14.34	10.43	7.93	0.38	2.11	0.93	0.16	0.95	0.57

FeO^{tot} is total iron expressed as FeO. Oxygen = O, which combines with FeO via the equation $2FeO + O = Fe_2O_3$; thus, bulk O is identically equal to bulk Fe_2O_3, while true bulk FeO is given by $FeO^{tot} - 2 \times O$. $X_{Mg} = MgO/(MgO + FeO^{tot})$. See text for the sources of the bulk-rock compositions.

Author Manuscript

Author Manuscript

Table 2. Modeled major (normalized wt%) and trace-element compositions (μg/g) of modeled melts along the Nankai geotherm.

Fresh MORB								**Altered OC**					
P–T (kbar, °C)	16.5, 690	17, 700	17, 710	17.5, 720	18, 730	18.5, 740	19, 750	17, 700	17, 710	17.5, 720	18, 730	18.5, 740	19, 750
wt %													
SiO_2	72.75	72.63	72.47	72.32	72.16	71.99	71.82	72.73	72.55	72.36	72.17	71.98	71.79
Al_2O_3	16.79	16.93	17.08	17.24	17.41	17.58	17.76	16.76	16.91	17.07	17.23	17.41	17.59
FeO	0.07	0.07	0.07	0.07	0.07	0.07	0.07	0.07	0.07	0.07	0.07	0.07	0.07
MgO	0.02	0.02	0.03	0.03	0.03	0.03	0.03	0.03	0.03	0.03	0.03	0.03	0.03
CaO	1.38	1.44	1.50	1.56	1.62	1.68	1.75	1.55	1.62	1.69	1.76	1.83	1.91
Na_2O	6.45	6.52	6.54	6.55	6.56	6.56	6.55	5.96	5.90	5.86	5.81	5.76	5.71
K_2O	2.55	2.39	2.31	2.23	2.15	2.08	2.02	2.90	2.92	2.93	2.93	2.92	2.90
Total	100.00	100.00	100.00	100.00	100.00	100.00	100.00	100.00	100.00	100.00	100.00	100.00	100.00
μg/g													
La	23.05	23.32	23.96	24.66	25.45	26.36	27.44	14.12	14.45	15.07	15.79	16.66	17.74
Ce	41.06	42.11	43.70	45.52	47.64	50.15	53.25	27.28	28.46	30.11	32.09	34.59	37.85
Pr	4.18	4.32	4.50	4.72	4.98	5.29	5.68	3.34	3.52	3.75	4.04	4.40	4.88
Nd	15.84	16.47	17.28	18.24	19.39	20.81	22.63	13.56	14.43	15.52	16.89	18.71	21.23
Sm	2.82	2.87	2.94	3.02	3.11	3.22	3.34	2.42	2.49	2.56	2.65	2.76	2.89
Eu	1.11	1.12	1.14	1.16	1.18	1.21	1.24	0.91	0.93	0.94	0.96	0.99	1.01
Gd	2.28	2.23	2.20	2.18	2.15	2.12	2.10	1.82	1.80	1.77	1.74	1.72	1.69
Tb	0.33	0.31	0.30	0.29	0.29	0.28	0.27	0.26	0.25	0.24	0.24	0.23	0.22
Dy	1.78	1.68	1.60	1.53	1.46	1.39	1.33	1.22	1.16	1.11	1.06	1.02	0.97
Ho	0.32	0.30	0.28	0.27	0.25	0.24	0.23	0.22	0.21	0.20	0.19	0.18	0.17
Er	0.83	0.77	0.72	0.67	0.63	0.59	0.55	0.53	0.50	0.47	0.44	0.42	0.39
Tm	0.12	0.11	0.10	0.09	0.09	0.08	0.08	–	–	–	–	–	–
Yb	0.71	0.65	0.60	0.55	0.52	0.48	0.45	0.44	0.41	0.38	0.36	0.34	0.31
Lu	0.10	0.09	0.09	0.08	0.07	0.07	0.06	0.07	0.06	0.06	0.05	0.05	0.05
Y	9.54	8.95	8.46	8.01	7.59	7.19	6.82	6.39	6.07	5.77	5.48	5.21	4.95
Sr	601	613	635	659	687	719	759	762	790	834	887	952	1037
Sr/Y	63	69	75	82	90	100	111	119	130	145	162	183	209
La/Yb	33	36	40	44	49	55	61	32	35	39	44	50	56